American Mineralogist, Volume 76, pages 1510–1532, 1991

Alpha-decay event damage in zircon

Takashi Murakami
Department of Environmental Safety Research, Japan Atomic Energy Research Institute, Tokai-Mura, Naka-Gun, Ibaraki-Ken, Japan

Bryan C. Chakoumakos
Solid State Division, Oak Ridge National Laboratory, Oak Ridge, Tennessee 37831, U.S.A.

Rodney C. Ewing
Department of Geology, University of New Mexico, Albuquerque, New Mexico 87131, U.S.A.

Gregory R. Lumpkin
Advanced Materials Program, Australian Nuclear Science and Technology Organisation, Private Mailbag 1, Menai 2234, New South Wales, Australia

William J. Weber
Pacific Northwest Laboratory, Richland, Washington 99352, U.S.A.

Abstract

Based on density measurements, X-ray diffraction analysis, and high-resolution transmission electron microscopy of a suite of natural zircon samples from Sri Lanka (0.06×10^{15} to 6.8×10^{15} α-decay events/mg), three stages of damage accumulation may be delineated. Stage I ($<3 \times 10^{15}$ α-decay events/mg) is characterized by sharp Bragg diffraction maxima with a minor contribution from the diffuse-scattering component. Electron diffraction patterns were sharp. Damage is dominated by the accumulation of isolated point defects, which cause unit-cell expansion and distortion that account for most of the decrease in density. These defects may partially anneal over geologic periods of time. Stage II (3×10^{15} to 8×10^{15} α-decay events/mg) is characterized by significant decreases in the intensity of the Bragg diffraction maxima, which become asymmetric from increased contributions of the diffuse-scattering component. High-resolution transmission electron microscopy indicated that the microstructure consists of distorted crystalline regions and amorphous "tracks" caused by α-recoil nuclei. With increasing α-decay dose, damaged crystalline regions are converted into aperiodic regions but with no further significant expansion of the unit cell in the remaining crystalline regions. Stage III ($>8 \times 10^{15}$ α-decay events/mg) consists of material that is entirely aperiodic as far as can be determined by X-ray or electron diffraction. There was no evidence for the formation of ZrO_2 or SiO_2 as final products during the last stage of metamictization. Based on modeled density changes, aperiodic regions continue to experience a change in structure as they are redamaged. During stage II of the process, the modeled density of aperiodic regions changes from 4.5 g/cm^3 to 4.1 g/cm^3. Fission fragment damage does not contribute to the process of metamictization. The amorphization process is consistent with a model for the multiple overlap of displacement cascades, suggesting amorphization occurs as a result of defect accumulation rather than directly within a single displacement cascade.

Comparison of results for natural zircon with those for Pu-doped zircon showed that dose-rate variations (even as great as a factor of 10^8) had no substantial effect on the damage accumulation process. Unit-cell parameters increased and density decreased more for the Pu-doped zircon than for natural zircon in the early stages of damage accumulation ($<3 \times 10^{15}$ α-decay events/mg), suggesting that annealing of point defects in the early stages of the damage accumulation process occurs in natural zircon under ambient conditions. This accounts for the distinct sigmoidal shape of the damage curves for natural zircon and the apparent incubation period before the onset of amorphization.

Introduction

Zircon ($ZrSiO_4$, $I4_1/amd$, $Z = 4$) is a common accessory mineral in crustal igneous, metamorphic, and sedimentary rocks, as well as in lunar materials, meteorites, and tektites. Because zircon typically contains 5 to 4000 ppm U and 2 to 2000 ppm Th (Ahrens et al., 1967; Gorz, 1974), it is one of the most important phases used in U-Th-Pb dating techniques (Faure, 1977; Jäger and Hunziker, 1979). Of particular interest are processes by which the U-Th-Pb systematics are disturbed (e.g., Silver and

0003–004X/91/0910–1510$02.00

Deutsch, 1963; Silver, 1964; Pidgeon et al., 1966; Steiger and Wasserburg, 1966; Davis et al., 1968; Suzuki, 1987). The structure of zircon is changed by α-decay damage associated with radioactive decay of naturally occurring radionuclides and their daughter products in the ^{238}U, ^{235}U, and ^{232}Th decay series. This process, metamictization (Ewing et al., 1987), can lead to increased solubilities (Ewing et al., 1983; Tole, 1985) and fracturing (Peterman et al., 1986; Chakoumakos et al., 1987), both of which can effect the U-Th-Pb systematics.

In addition, the zircon structure type is an actinide-bearing phase in proposed crystalline, polyphase, ceramic nuclear waste forms (Harker and Flintoff, 1984), and natural zircon has been used to evaluate elemental loss from waste-form phases under repository conditions (Gentry et al., 1982; Ludwig et al., 1984; Gentry, 1984). For this reason, an important area of research has been the comparison of radiation damage effects in Pu-doped, tetragonal monosilicates (Exarhos, 1984; Weber and Maupin, 1988; Weber, 1990, 1991) with those observed in natural zircon. This comparison allows for the determination of dose-rate effects (which differ by a factor of 10^8) and long-term annealing kinetics under ambient conditions.

We present results of a study of a suite of natural zircon samples from Sri Lanka that span a range of doses (10^{13} to 10^{15} α-decay events/mg) over which the transition from the crystalline to aperiodic, metamict state occurs. These results for natural zircon are compared with data obtained (1) on a Pu-doped zircon sample that has attained doses on the order of 10^{16} α-decay events/mg (Exarhos, 1984; Weber and Maupin, 1988; Weber, 1990, 1991); (2) on ion-implanted zircon [Ar and Kr at 1–3.5 MeV up to 10^{15} ions/cm^2 (Cartz and Fournelle, 1979), Pb at 40–240 keV up to 10^{13} Pb/cm^2 (Headley et al., 1982), Pb at approximately 230 keV up to 10^{15} Pb/cm^2 (Petit et al., 1987), and Pb at 14 MeV at 10^{11} Pb/cm^2 (Bursill and Braunshausen, 1990)]; and (3) for fast neutron irradiations [up to 3.6×10^{20} neutrons/cm^2 (Crawford and Wittels, 1956)]. For the ion implantation, the transition from the crystalline to the metamict state occurs in the fluence range of 10^{13} to 10^{15} ions/cm^2. For the fast neutron irradiations, considerable long-range periodicity is still preserved at the maximum fluxes ($>10^{20}$ neutrons/cm^2, $E_n > 50$ keV). The comparison of natural zircon samples with those irradiated over relatively short periods of time (up to 6.5 yr for the Pu-doped zircon sample) allows the determination of whether annealing of radiation damage occurs over geologic periods of time.

Previous work

There is extensive literature on the crystal chemistry, radiation damage, dissolution mechanisms, and alteration processes for natural and synthetic zircon. This review of previous work is not comprehensive but rather is designed to focus the discussion of our results on critical questions related to the radiation-induced transformation of zircon from the crystalline to the metamict (aperiodic) state, as revealed mainly by density, X-ray diffraction (XRD), and high-resolution transmission electron microscopy (HRTEM).

Hamberg (1914) was the first to suggest that metamictization is a radiation-induced, periodic-to-aperiodic phase transition caused by α particles that originate from constituent radionuclides in the U and Th decay series. Stackelberg and Rottenback (1940a, 1940b) related changes in properties, e.g., density and refractive indices, to the breakdown of the periodic structure, and they tried to confirm this hypothesis in an inconclusive effort by bombarding a thin slab of zircon with α particles. This is probably the first experiment in which an ion beam was used in an attempt to modify a ceramic material. We now recognize that α-decay damage is caused by two separate, simultaneous processes associated with the α-decay event: (1) An α particle (4.5 to 5.0 MeV) with a range of 10000 nm dissipates most of its energy by ionization; however, at low velocities near the end of its track, it displaces several hundred atoms creating isolated Frenkel defect pairs; (2) the α-recoil atom (0.07–0.09 MeV) with a range of 10 nm produces several thousand atomic displacements creating "tracks" of disordered material. These two damaged areas are separated by thousands of unit-cell distances (e.g., the c cell edge for zircon is 0.60 nm), and the two processes have different effects on the crystalline structure (Weber, 1981, 1984).

The broader interest in radiation damage effects in zircon developed after the suggestion by Holland and Kulp (1950) and Hurley and Fairbairn (1952, 1953) that the accumulation of radiation damage in zircon, measured by shifts in diffraction maxima, could be used to age date geologic materials. The refinement of their ideas came with the classic paper by Holland and Gottfried (1955) in which they studied changes in density, refractive index, and unit-cell parameters for a suite of zircon samples from Ceylon that reached doses of approximately 10^{16} α-decay events/mg. Holland and Gottfried quantitatively documented the dramatic changes in properties over a narrow range of α-decay event dose from 10^{15} to 10^{16} α-decay events/mg: (1) a 16% decrease in density (reaching saturation at 1.1×10^{16} α-decay events/mg), (2) a decrease in refractive indices to a single value (1.84) with the complete loss of birefringence (at a dose of 1.34×10^{16} α-decay events/mg), (3) the anisotropic expansion of the unit cell ($c > a$), and (4) a 5.2% increase in unit-cell volume until the material became X-ray diffraction amorphous (at 4.5×10^{15} α-decay events/mg). They proposed three stages for the damage process including an intermediate, crystalline phase (phase 2), leading finally to the formation of a glass. The structural arrangement of the intermediate phase "crystallites" was considered critical to the continued damage accumulation process. The crystallites either recrystallized to the original matrix, if aligned to the residual structure, or continued to break down to form a glass, if the crystallites were disoriented. The experimental approach in their study is essentially the same as that used in this study, but the application of some additional analytical techniques (HRTEM)

leads to a substantial increase in our understanding of this radiation-induced transformation.

Since 1955, there has been considerable research on zircon, both crystalline and metamict. Pabst (1952), Ewing (1975), Speer (1982), Ewing et al. (1987), and Chakoumakos et al. (1987) summarized the effects of α-decay damage on zircon: (1) decrease in density (17%), (2) decrease in refractive indices and birefringence until isotropic, (3) darkening of color, (4) decrease in intensity and broadening of optical and infrared absorption bands which become isotropic, (5) increasing thermoluminescence, (6) broadening, decrease in intensity, and shift in the position of diffraction maxima to lower values of 2θ, which corresponds to an increase in unit-cell volume (5%), (7) decrease in elastic modulus (70%), (8) decrease in hardness (40%), (9) decrease in Poisson's ratio (7%), (10) decrease in thermal conductivity, (11) increase in adsorbed H_2O, (12) increased susceptibility to dissolution, and (13) increased chemical diffusion.

Analytical techniques

Density

Densities were measured on fragments (15–25 mg) using a Berman balance. Carbon tetrachloride was the immersion medium, and no corrections were made for liquid volume expansion as a function of temperature because the amounts were negligible.

Instrumental neutron activation analysis (INAA)

U and Th concentrations of the 18 samples were measured by instrumental neutron activation analysis (Minor et al., 1982). Gamma-ray spectroscopy was used to measure Th concentrations. The delayed neutron counting technique, which counts delayed neutrons from the fission of ^{235}U, was used for the measurement of U concentrations assuming a natural abundance for ^{235}U of 0.72%. Standards used were the U.S. Geological Survey Glass Mountain rhyolite and the U.S. Geological Survey analyzed nepheline syenite.

Electron microprobe analysis (EMPA)

Polished sections of the zircon crystals were analyzed for as many as nine elements simultaneously with a JEOL 733 Superprobe operated at 14 kV with a beam diameter of 2 μm. The detection limits and precision for minor elements were improved by using a sample current of 50 nA with counting times of up to 90 s for U and Th. Minimum detection limits were approximately 100 ppm for Al, P, Ca, and Y; 150 ppm for Th and U; and 200 ppm for Ce. Data were corrected for dead time, drift, fluorescence, and absorption effects by using an empirical α-factor approach (Bence and Albee, 1968; Albee and Ray, 1970). Standards included synthetic zircon (for Si, Zr, and Hf), synthetic thorite (for Th), YPO_4 (for Y), $CePO_4$ (for Ce and P), UO_2 (for U), and anorthite (for Al and Ca).

XRD

Powder X-ray diffraction was used to examine general changes in whole patterns and peak profiles for six of the 18 samples, and powder diffraction data were used to refine unit-cell parameters for all 18 samples. Data were obtained on a Scintag Pad V automated diffractometer (Cu$K\alpha$, with a diffracted-beam graphite monochromator) using BaF_2 as an internal standard. The 200 diffraction maximum was used for the profile analysis instead of the 112 maximum in order to avoid complications from the resolution of the $K\alpha$ doublet at higher values of 2θ (Holland and Gottfried, 1955; Bursill and McLaren, 1966). Howard and Sabine (1974) have shown that the asymmetry of radiation damaged materials results from diffuse scattering caused by interstitial defects. The diffuse scattering occurs on the high-2θ side of the Bragg diffraction maximum. The 200 diffraction maximum was decomposed into a Bragg diffraction maximum and the diffuse-scattering component using a least-squares fit to a Pearson VII function. The 2θ values for the peak positions and the full width at half maximum (FWHM) were obtained from the least-squares fitted values. The peak intensity was determined by integration. For the cell-parameter refinements, Bragg maxima positions were determined using a least-squares fit after decomposition of the diffraction maxima into Bragg and diffuse components. Cell parameters were refined based on the decomposed Bragg peak positions (Appleman and Evans, 1973). Selected cell parameters were also calculated without decomposition. (The entire diffraction maximum with the diffuse-scattering component included was used to determine peak position.) The precession method (Mo$K\alpha$, Zr filter) was used on selected samples for the comparison of X-ray diffraction patterns with electron diffraction patterns.

HRTEM

Crushed samples dispersed onto holey carbon–coated copper grids in methanol were examined with a JEOL 2000 FX analytical electron microscope operated at 200 kV. Bright field (BF), selected area diffraction (SAD), and high-resolution (HRTEM) techniques were used. The HRTEM images were taken at a magnification of 410 000. In situ heating experiments were carried out with a heating stage up to temperatures of 750 °C. SAD patterns were analyzed before and after the annealing experiments.

Sample description

Approximately 200 crystals of zircon were obtained by R.C.E. from the gem gravels of the Ratnapura district in Sri Lanka. The samples were collected from workers in the field in order to prevent any heat treatment of the zircon. The occurrence of zircon in Ratnapura is described well by Munasinghe and Dissanayake (1981), Dahanayake and Ranasinghe (1981), and Kröner et al. (1987). The zircon is remarkably consistent in its age, as indi-

TABLE 1. Average electron microprobe analyses and formulas

	4403	4606	4603	4602	4303	4501	4601	4304	4103	4104
P_2O_5	0.06	0.07	0.08	0.10	0.11	0.07	0.06	0.10	0.08	0.11
SiO_2	32.0	31.4	31.6	30.5	31.9	32.1	31.5	31.2	31.7	31.5
ZrO_2	67.8	67.8	66.0	68.0	66.1	64.4	65.8	64.9	65.8	64.6
HfO_2	0.95	1.10	1.26	1.01	1.12	1.95	1.16	1.30	1.21	2.26
ThO_2	0.00	0.01	0.01	0.05	0.03	0.12	0.06	0.10	0.08	0.11
UO_2	0.01	0.13	0.11	0.13	0.16	0.35	0.29	0.26	0.38	0.31
Al_2O_3	0.02	0.02	0.01	0.01	0.01	0.02	0.00	0.01	0.02	0.01
Y_2O_3	0.01	0.07	0.06	0.10	0.17	0.09	0.10	0.24	0.23	0.15
Ce_2O_3	0.00	0.01	0.02	0.01	0.02	0.00	0.03	0.01	0.04	0.01
CaO	0.00	0.01	0.00	0.00	0.00	0.00	0.00	0.01	0.00	0.00
Total	100.85	100.62	99.15	99.91	99.62	99.10	99.00	98.13	99.54	99.06
P	0.002	0.002	0.002	0.003	0.003	0.002	0.002	0.003	0.002	0.003
Si	0.977	0.966	0.982	0.950	0.986	0.998	0.983	0.983	0.984	0.986
Al	0.001	0.001	0.000	0.000	0.000	0.001	0.000	0.000	0.001	0.000
B Site	0.980	0.969	0.984	0.953	0.989	1.001	0.985	0.986	0.987	0.989
Zr	1.012	1.018	1.002	1.034	0.997	0.977	1.001	0.996	0.997	0.986
Hf	0.008	0.010	0.011	0.009	0.010	0.017	0.010	0.012	0.011	0.20
Th	0.000	0.000	0.000	0.000	0.000	0.001	0.000	0.001	0.001	0.001
U	0.000	0.001	0.001	0.001	0.001	0.002	0.002	0.002	0.003	0.002
Y	0.000	0.001	0.001	0.002	0.003	0.001	0.002	0.004	0.004	0.003
Ce	0.000	0.000	0.000	0.000	0.000	0.000	0.000	0.000	0.000	0.000
Ca	0.000	0.000	0.000	0.000	0.000	0.000	0.000	0.000	0.000	0.000
A Site	1.020	1.030	1.015	1.046	1.011	0.998	1.015	1.015	1.016	1.012

Note: O = 4.00.

cated by independent age determinations on over 20 separate crystals (Gottfried et al., 1956). The average age is taken as 570 ± 20 m.y. to facilitate direct comparison with results of Holland and Gottfried (1955). Individual crystals vary in size from 3 to 15 mm in their longest dimension and are euhedral, prismatic, and slightly rounded by stream transport. The colors vary from dark orange to brown, orange, green, black, and dark green, a sequence of color changes that roughly corresponds to increasing radiation damage. No evidence suggests metamorphic deformation or chemical alteration. The zircon is thought to be derived from granitic plutons and pegmatites. Based on their gem quality and lack of any apparent alteration or heterogeneities, 18 crystals were selected for this study.

Average compositions of ten zircon samples are listed in Table 1 together with structural formulas calculated on the basis of 4.0 O atoms per formula unit. The zircon samples are of near end-member composition. The major elemental impurity in all the samples is Hf. The average amount of HfO_2 ranges from 0.95 to 2.26 wt% for the ten specimens, equivalent to 0.8–2.0 mol% of the $HfSiO_4$ end-member. Other significant minor elements are P, Th, U, and Y. Maximum average concentrations of these elements, expressed as oxides, are 0.11 wt% P_2O_5, 0.12 wt% ThO_2, 0.38 wt% UO_2, and 0.24 wt% Y_2O_3. These values correspond to maximum average end-member components of 0.4 mol% YPO_4, 0.3 mol% $USiO_4$, and only 0.1 mol% $ThSiO_4$. Concentrations of the minor components are so low as to have a negligible effect on unit-cell parameters. Consequently, essentially all the variation in unit-cell parameters between samples is related to α-decay damage resulting from their U and Th contents (Table 2).

The amounts of Al, Ce, and Ca listed in Table 1 are near the minimum detection limits in most of the zircon samples. In particular, the amount of Ca is at or below the minimum detection limit in all ten samples. This result indicates that the samples are virtually unaltered, as Ca is one of the most common indicators of alteration of zircon and thorite (Wayne and Sinha, 1988; Lumpkin and Chakoumakos, 1988). Intracrystalline variations in composition are mainly related to lamellar zoning observed in six of the specimens. The major variation from

TABLE 2. U and Th concentrations, α-decay doses, and densities of Sri Lankan zircon samples

Sample no.	U (ppm)	Th (ppm)	Dose* ($\times 10^{15}$ α/mg)	Dose** ($\times 10^{15}$ α/mg)	Density (g/cm³)
4403	26 ± 4	31 ± 5	0.06(1)†	0.05	4.72
4407	35.8 ± 3.7	10.9 ± 2.3	0.075(8)	0.072	4.69
4606	712 ± 33	137.7 ± 9.6	1.46(7)	1.43	4.65
4603	900 ± 40	330 ± 10	1.92(8)	1.81	4.59
4602	942 ± 43	363 ± 17	2.01(9)	1.90	4.62
4605	989 ± 44	204 ± 12	2.04(9)	1.99	4.58
4607	979 ± 44	394 ± 20	2.1(1)	2.0	4.59
4303	890 ± 40	810 ± 50	2.1(1)	1.8	4.58
4604	1680 ± 76	496 ± 23	3.5(2)	3.4	4.54
4302	2069 ± 93	283 ± 17	4.2(2)	4.2	4.40
4601	2200 ± 100	590 ± 20	4.6(2)	4.4	4.38
4204	2520 ± 110	602 ± 34	5.2(2)	5.1	4.40
4501	2560 ± 120	898 ± 44	5.4(3)	5.2	4.35
4304	2640 ± 120	1340 ± 70	5.8(3)	5.3	4.36
4105	3040 ± 140	702 ± 39	6.3(3)	6.1	4.25
4104	3010 ± 140	969 ± 46	6.4(3)	6.1	4.24
4103	3160 ± 140	1140 ± 60	6.7(3)	6.4	4.17
4102	3210 ± 140	1073 ± 47	6.8(3)	6.5	4.27

* Calculated on basis of measured U and Th concentrations (this study) and on an age of 570 m.y.

** Calculated assuming U/Th = 9/1 and an age of 570 m.y. (Holland and Gottfried, 1955).

† Error for last digit is given in parentheses.

TABLE 3. Birefringence variations determined by optical microscopy and U concentration variations determined by electron microprobe analysis and bulk α-decay event doses and densities

Sample no.	Bulk dose ($\times 10^{15}$ α/mg)	Bulk density (g/cm^3)	Range of birefringence	Range of calculated density (g/cm^3)*	Range of U concentration (wt%)
4403	0.06	4.72	0.040–0.070	4.51–4.83	0–0.03
4606	1.46	4.65	0.035–0.050	4.45–4.61	0.10–0.15
4603	1.92	4.59	0.045–0.055	4.56–4.67	0.07–0.15
4602	2.01	4.62	0.040–0.055	4.51–4.67	0.09–0.13
4303	2.1	4.58	0.017–0.020	4.26–4.29	0.09–0.17
4601	4.6	4.38	0.008–0.045	4.16–4.56	0.17–0.40
4501	5.4	4.35	0.018–0.036	4.27–4.46	0.24–0.46
4304	5.8	4.36	0.006–0.008	4.14–4.16	0.20–0.26
4104	6.4	4.24	0.008–0.010	4.16–4.18	0.26–0.30
4103	6.7	4.17	0.008–0.020	4.16–4.29	0.29–0.40

* Density = 4.078 + 10.678 (birefringence) (Sahama, 1981).

zone to zone is in the amount of U (Table 3). Lesser variations in the amounts of Th, Y, and P are present, but these elements consistently show a positive correlation with U (see Chakoumakos et al., 1987). Data in Table 3 also show that two unzoned samples, 4303 and 4603, have significant ranges of U concentration. Compositional profiles of these samples exhibit broad, irregular variations in U content. Zircon sample 4603, for example, has an asymmetric U profile with the highest U values skewed to one side of the core of the crystal and low to moderate U contents in the rim.

Structural formulas give in Table 1 show that eight of ten zircon samples are within ± 2 mol% of ideal ABO_4 stoichiometry. The other two samples, 4606 and 4602, have somewhat lower B-site totals of 0.97 and 0.95 atoms per formula unit, respectively. However, these lower values may not be significant as the B-site totals in general appear to be systematically low by 1–2 mol%. Together with analytical totals in the range of 98–101 wt%, structural formulas suggest that the substitution $4H^+ \rightarrow Si^{4+}$ is limited to trace levels in the Sri Lankan samples. This is another clear indication of the general absence of alteration in these samples; however, we cannot rule out the possibility of trace amounts of H_2O associated with radiation damage sites (Aines and Rossman, 1986).

Despite any evidence of heterogeneity or zoning in hand specimens, some crystals show dramatic growth zoning on the scale of tens to hundreds of micrometers (Chakoumakos et al., 1987; Woodhead et al. 1991). Of the samples selected for detailed study, six showed distinct zoning when they were examined in thin section. This type of zoning is apparently common among the gem zircon samples from the gravels of Ratnapura and has been described in detail by Sahama (1981) and Chakoumakos et al. (1987). The zonation is manifest in dramatic variations in birefringence (Table 3), which are caused by variations in α-decay damage resulting from variable U and Th contents. With increasing α-decay dose, both refractive indices decrease until they reach the same saturation value (1.81) and the material becomes optically isotropic (Holland and Gottfried, 1955). U and Th concentrations from electron microprobe analyses can be correlated with the birefringence (Sahama, 1981; Chakoumakos et al., 1987). This means that, properly calibrated, birefringence can be used to estimate the α-decay dose. Densities of individual layers can be determined from the dose calculated from the measured ranges of U concentrations (EMPA). The range of inferred densities may also be calculated from Sahama's (1981) relation:

$$\text{density} = 4.078 + (10.678)\,(\text{birefringence}). \quad (1)$$

Despite the wide ranges of α-decay event dose, density, and birefringence shown by the zoned crystals, the ranges and means of these values fall close to the line for the measured bulk density and bulk α-decay dose (based on INAA analysis for U and Th). As an example, sample 4601 (Fig. 1) has the widest range of density (inferred from birefringence), yet the average value is nearly that expected from the determined bulk density and bulk α-decay event dose. Concentrations of Th, Y, and P vary sympathetically with the U, but the concentrations are much less (generally <0.1 wt% for ThO_2) and the relative range of variation is less.

Thus, individual zoned crystals can be used to measure bulk changes in property with progressive damage. This is well illustrated in the study by Holland and Gottfried (1955) in which some of their Sri Lankan zircon samples must have also been zoned (see Sahama, 1981; Woodhead et al., 1991). Optical properties were determined by an immersion method and would have provided an average value for the refractive indices. The position of X-ray diffraction maxima will also represent average bulk values, but the asymmetry of the peaks shown in Holland and Gottfried (1955) may be the result of overlap of multiple peak positions caused by the zoning. The zoning will, however, cause complexities in interpreting the X-ray and electron diffraction data.

Alpha-decay event dose calculation

An α-decay dose was calculated for each sample based on the U and Th concentrations by the equation (Holland and Gottfried, 1955)

$$D = 8N_1[\exp(a_1 t) - 1] + 7N_2[\exp(a_2 t) - 1] + 6N_3[\exp(a_3 t) - 1] \quad (2)$$

where D is the dose in α-decay events/mg; N_1, N_2, and N_3 are the present numbers of ^{238}U, ^{235}U, and ^{232}Th, respectively, in atoms/mg; a_1, a_2, and a_3 are the decay constants for ^{238}U, ^{235}U, and ^{232}Th, respectively, in years^{-1}; and t is the age of the zircon, 570 m.y. N_2 is assumed to be equal to $(1/139)N_1$ based on natural abundances. In comparing our calculated α-decay doses with those of Holland and Gottfried (1955), one should note that they assumed a high U/Th ratio of 9 for all of the Sri Lankan zircon samples. In contrast, we independently measured Th concentrations and found that in some cases the Th content was substantial. In the case of the high-Th zircon

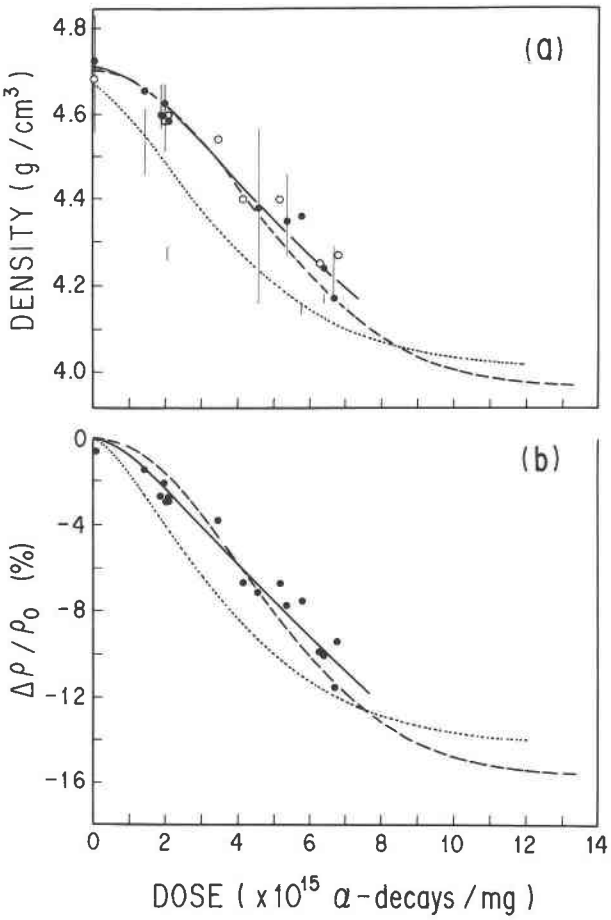

Fig. 1. (**a**) Plot of the change in density of zircon with increasing α-decay dose. The solid line is for samples in this study, and vertical bars indicate the range of densities in zoned samples (this study) based on the measurement of birefringence (solid circles = birefringence measured; open circles = birefringence not measured). The zoned sample with the broadest range of densities is 4601. The dashed line represents the data of Holland and Gottfried (1955); the dotted line, data for Pu-doped zircon (Weber, 1990). (**b**) Plot of $\Delta\rho/\rho$ of zircon with increasing α-decay dose from this study, the work of Holland and Gottfried (1955), and for Pu-doped zircon (Weber, 1990).

samples, our calculated doses will be higher (see Table 2 for comparison).

Results

Density

Based on the measurements of Holland and Gottfried (1955), the range of density values for samples in this study, 4.72–4.17 g/cm^3, corresponds to α-decay doses that span nearly the full range of required dose for the periodic to aperiodic transition (Table 2). None of the samples reaches a saturation value (3.9 g/cm^3) characteristic of fully damaged material. Density as a function of α-decay event dose is shown in Figure 1a. There is excellent agreement between our results and those of Holland and Gottfried (1955) below an α-decay dose of 3×10^{15} α-decay events/mg. At higher doses, our calculated dose at any given density is slightly higher. This is because we have calculated the dose from measured (generally higher) values for the ^{232}Th contents, and these values contribute to the total α-decay dose. The highest dose for any of our samples is 6.8×10^{15} α-decay events/mg; thus, none of our samples reaches a saturation value for the decrease in density that is expected at a dose of approximately 10^{16} α-decay events/mg.

Table 4. Volume- and density-change parameters for natural and Pu-doped zircon

Material	A_ρ (%)	B_ρ (g)	n
Unit-cell volume			
Natural zircon (this study)	4.89	3.64×10^{-19}	1.70
Natural zircon (Holland and Gottfried, 1955)	5.06	3.92×10^{-19}	2.29
Pu-doped zircon (Weber, 1990)	5.10	3.45×10^{-19}	1.00
Density			
Natural zircon (this study)	−15.6	1.49×10^{-19}	1.60
Natural zircon (Holland and Gottfried, 1955)	−15.6	1.70×10^{-19}	2.03
Pu-doped zircon (Weber, 1990)	−14.2	2.29×10^{-19}	1.41

If we compare our data with those for Pu-doped zircon (Fig. 1a), the decrease in density is greater for the Pu-doped zircon than for natural zircon. The position of the curve for samples in this study compared with that of Holland and Gottfried (1955) only accentuates this difference. Another important feature is the difference in the shape of the curves, most pronounced at low doses (<6 $\times 10^{15}$ α-decay events/mg), suggesting recovery of isolated defects in the structure of natural zircon. At higher doses (>6 $\times 10^{15}$ α-decay events/mg), the difference in the positions of the curves is less pronounced. In this damage regime, density changes are dominated by the metamictization associated with the accumulation of α-recoil tracks. Here structural recovery is limited, as most of the volume is already aperiodic.

The change in density with increasing dose in both natural and Pu-doped zircon is sigmoidal. The relative change in the measured density, $\Delta\rho/\rho$, as a function of cumulative dose provides a convenient comparison of the behavior for the Pu-doped and natural zircon because this reduces the effect of the 5.5% porosity of the synthetic, Pu-doped zircon. In both the Pu-doped and natural zircon, the $\Delta\rho/\rho$ data (Fig. 1b) follow sigmoidal behavior that is approximated by an empirical expression of the form

$$\Delta\rho/\rho = A_\rho\{1 - \exp[-(B_\rho D)^n]\} \quad (3)$$

where A_ρ is the relative density change at saturation, B_ρ is related to the mass of material damaged per decay event, and n is an order parameter that produces sigmoidal rather than simple exponential behavior. The parameters A_ρ, B_ρ, and n, which were determined by nonlinear regression analysis, are given in Table 4. Sigmoidal behavior of the density change has not been previously observed in studies of amorphization in other actinide-doped materials

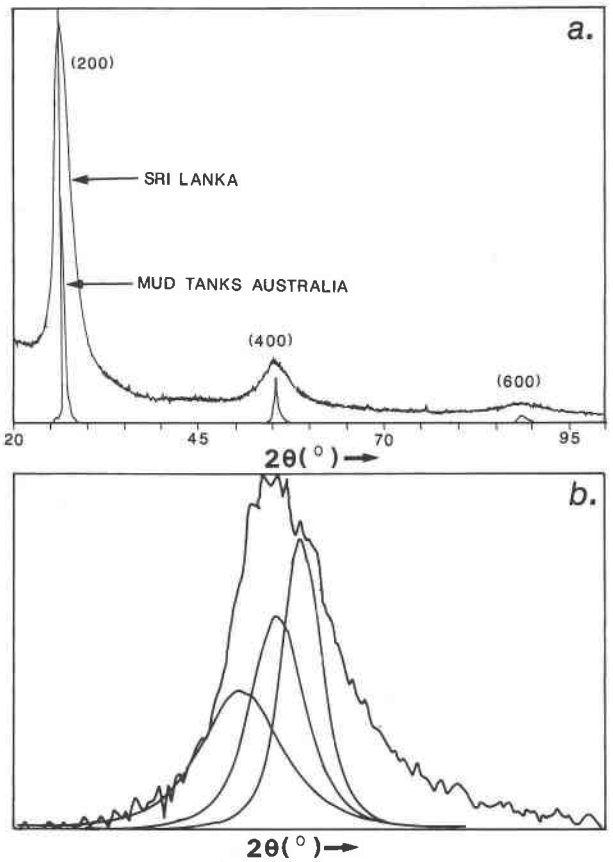

Fig. 2. (a) An XRD (Cu$K\alpha$) θ-2θ scan of zircon (100) single-crystal sections. The scan intensity for sample 4601 has been scaled to be equal to that of a highly crystalline zircon sample from Mud Tanks, Northern Territory, Australia. The line broadening results from the radiation damage in individual zones. The high background at the low-2θ side of 200 for 4601 is scattering from the crystal bond adhesive. (b) A schematic illustration of the effect of three overlapping peaks (e.g., from a zoned zircon sample) successively shifted to lower values of 2θ and broadened as a result of α-decay damage. The composite peak is skewed in the low-2θ direction. In contrast, the diffuse-scattering component occurs on the high-2θ side of the Bragg diffraction maximum.

(Weber, 1983; Weber et al., 1986; Weber and Matzke, 1986; Clinard, 1986); however, these other materials exhibited much smaller density decreases (only up to -8% as a result of the radiation-induced disorder and amorphization) than observed in zircon. Consequently, the sigmoidal character may not be evident except in cases in which the density changes associated with amorphization are large, such as in the amorphization of neutron-irradiated quartz where the density change decreases sigmoidally to a saturation value of -14.7% (Wittels and Sherrill, 1954).

X-ray diffraction analysis

The general features of the X-ray diffraction of patterns of zircon with increasing α-decay dose have been illustrated in Murakami et al. (1986). With increasing α-decay event dose, diffraction maxima decrease in intensity, shift to lower values of 2θ, broaden, and become asymmetric. The line broadening with increasing α-decay dose is commonly observed in metamict minerals and is typically asymmetric. The broadening is caused by interstitial defects in the early stages of the damage and decreasing grain size as the volume of the aperiodic regions increases (Lumpkin and Ewing, 1988). This is illustrated in the X-ray diffraction pattern for a partially damaged zircon sample, 4601, compared with highly crystalline zircon from Mud Tanks, Northern Territory, Australia (Fig. 2a). For zoned zircon, a component of the broadening must also be ascribed to the range of doses represented by individual zones in a single crystal and perhaps the strain induced by the differential expansion of the zones. Figure 2b illustrates the effect of overlapping peaks from zones of progressively increasing α-decay damage. These multiple peaks skew the composite peak to the low-2θ side of the peak. In contrast, the diffuse-scattering component will be on the high-2θ side of the diffraction maximum. For unzoned zircon the increasing asymmetry of the peak with increasing α-decay dose is a result of the combined effects of a decrease in the intensity of the Bragg diffraction maximum and an increase in the intensity of the diffuse-scattering component (on the high-2θ side of the Bragg maximum) associated with the aperiodic regions. The Bragg and diffuse-scattering component can be determined by decomposition of the single, broad diffraction maxima. This is illustrated for six samples in Figure 3. With increasing α-decay dose, the Bragg maximum shifts to lower values of 2θ, but the shift reaches a maximum value at doses of 3×10^{15} α-decay events/mg. (Note that the position of the Bragg component, dashed line, does not shift much for samples 4601, 4304, and 4103.) At the same time that the intensity of the Bragg diffraction maximum has decreased by 2 orders of magnitude, the intensity of the diffuse-scattering component increases until the two intensities are nearly equal at doses above 3×10^{15} α-decay events/mg. The FWHM for the Bragg maxima are three to six times greater above the dose of 3×10^{15} α-decay events/mg than for the more crystalline samples below this dose. The crystalline samples (4303, 4403, and 4603) show only minor diffraction maxima broadening.

Seven of the 18 samples show distinct peak splitting. Peak splitting was determined by examining peaks at 2θ values higher than 45° (Cu$K\alpha$). The peak profiles at high values of 2θ may be quite complicated because $K\alpha_1$ and $K\alpha_2$ peaks may be individually resolved. $K\alpha_1$ and $K\alpha_2$ can each in turn also be resolved into a Bragg and diffuse-scattering component; thus, in the presence of two phases, one may expect to see eight peaks. Figure 4 illustrates typical peaks for the 312 diffraction maximum. Sample 4403 is essentially crystalline (6.0×10^{13} α-decay events/mg) and shows normal $K\alpha_1$ and $K\alpha_2$ splitting (Fig. 4a). Sample 4303 is slightly more damaged (2.1×10^{15} α-decay events/mg) and has a complicated peak profile with

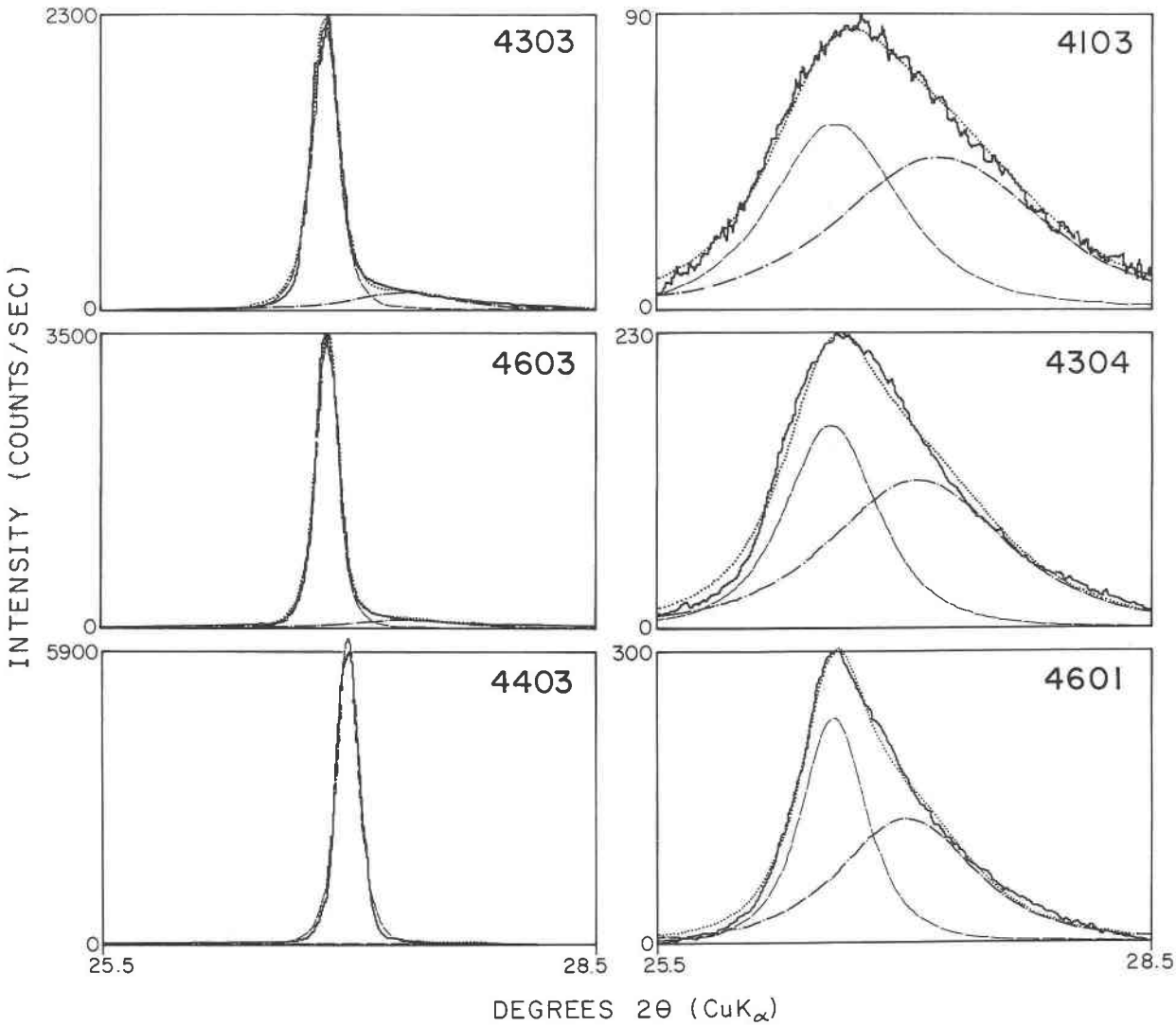

Fig. 3. Profiles of 200 peaks with increasing α-decay dose. Solid lines are the observed diffraction maxima; dots, calculated curves; dashed lines, Bragg diffraction components; dots and dashes, diffuse-scattering components (taken from Murakami et al., 1986). The α-decay event doses are given for each sample in Table 2.

three sharp peaks (A, B, and C) and a diffuse-scattering component (D) (Fig. 4b). The profile can be explained if one assumes two phases, I and II. Peaks A and B result from $K\alpha_1$ and $K\alpha_2$ of phase I; peaks B and C, from $K\alpha_1$ and $K\alpha_2$ of phase II. Thus, the intensity for peak B is the sum of the intensities of $K\alpha_2$ of phase I and $K\alpha_2$ of phase II. This assumption is consistent with the 2θ values and intensities of peaks A, B, and C for 4303 and the data for 4403 and 4601 (Table 5). The diffuse-scattering component (D) is the sum of the four diffuse-scattering components associated with $K\alpha_1$ and $K\alpha_2$ of phases I and II. As the α-decay damage increases, it is usually impossible to identify the number of contributing phases because of the low diffraction intensities and the severe line broadening (e.g., Fig. 4c, sample 4601, with a dose of 4.6×10^{15} α-decay events/mg). Figure 5a, showing a combination of peaks for sample 4604 (3.5×10^{15} α-decay events/mg), illustrates that peak splitting can be quite complicated. Peak A may be the sum of peaks for $K\alpha_1$ and $K\alpha_2$ of more than two phases; peaks B and C are $K\alpha_1$ and $K\alpha_2$ for another phase. The intensity ratio for peak B to C is not correct [see Table 6; if the intensity for B($K\alpha_1$) is correct, assuming only one phase contributes to B, then the intensity of C($K\alpha_2$) should be approximately 250] because the intensities of peaks B and C include contributions from the diffuse-scattering component of peak A and the intensity of peak C also includes a contribution from the diffuse-scattering component of peak B. Another extreme example is sample 4105 (6.3×10^{15} α-decay events/mg) in Figure 5b. Here one may imagine diffraction maxima from two phases, A and B; peak C may be the diffuse-scattering component associated with peak B.

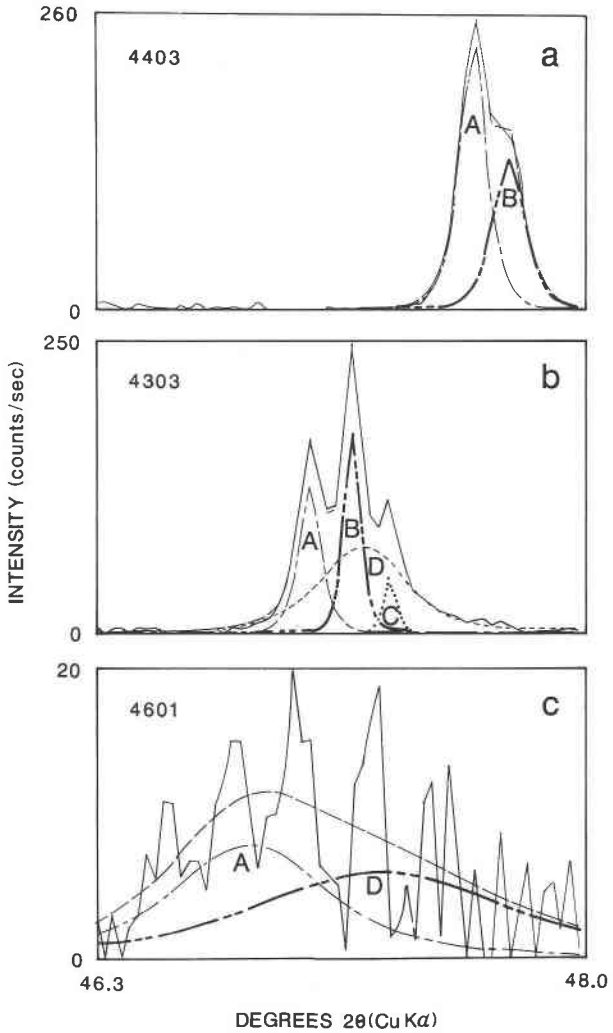

Fig. 4. Typical 312 diffraction maxima of zircon and decomposed peaks. (a) Sample 4403 is essentially crystalline (0.06 × 10^{15} α-decay events/mg); (b) 4303 (2.1 × 10^{15} α-decay events/mg); (c) 4601 (4.6 × 10^{15} α-decay events/mg). Data are given in Table 5.

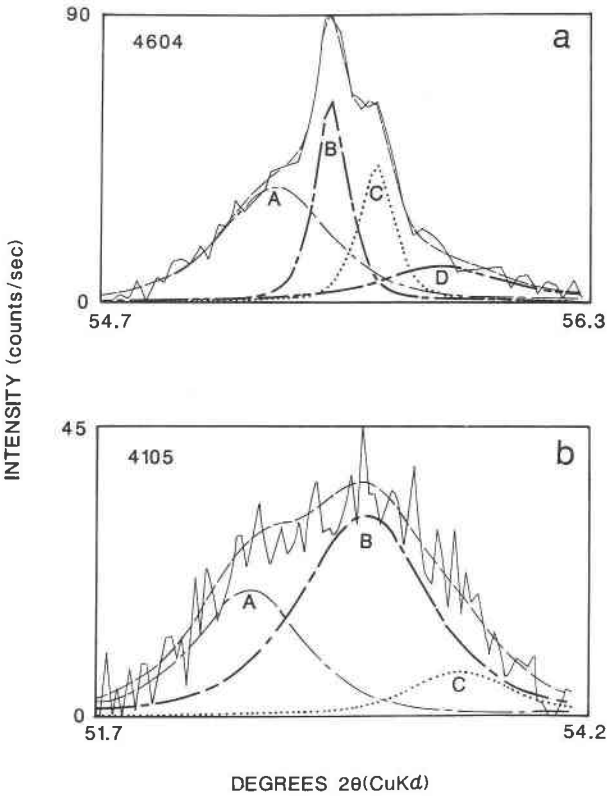

Fig. 5. Selected diffraction maxima of zircon and decomposed peaks. (a) Sample 4604 (3.5 × 10^{15} α-decay events/mg); (b) sample 4105 (6.3 × 10^{15} α-decay events/mg). Data are given in Table 6.

No further resolution is possible because of the low intensities and the severe line broadening.

Of the seven samples that show peak splitting, six fall in the dose range of 1 to 4 × 10^{15} α-decay events/mg (4606, 4602, 4605, 4303, 4607, and 4604), and five of the six range from 1 to 2 × 10^{15} α-decay events/mg. The only sample that shows peak splitting and falls outside this range of dose is 4105 (6.3 × 10^{15} α-decay events/mg). Note that samples with low α-decay event doses do not show peak splitting because the dose difference from zone to zone in a single sample is small. For example, 4403 (0.6 × 10^{14} α-decay events/mg) is zoned, but the maximum difference in dose between zones is 0.5 × 10^{15} α-decay events/mg. This α-decay event dose difference cannot cause a significant peak shift (see Figs. 6 and 7, which show the change in cell parameter as a function of α-decay dose). At high α-decay doses, the loss of diffraction intensity and the severe line broadening obscure any difference between individual zones. Thus peak splitting caused by variations in α-decay dose received by individual zones will only affect the X-ray diffraction results at intermediate α-decay doses. Table 7 compares results for samples that were examined by both optical microscopy and X-ray diffraction. Although zoned zircon was identified over the full range of α-decay doses for samples in this study, peak splitting is only evident at low or intermediate α-decay doses.

The most important data to be extracted from the X-ray diffraction analysis are the refined unit-cell parameters (Table 8). Initial refinements were made assuming only a single phase (that is, the sample was unzoned), and each diffraction maximum was decomposed into a single Bragg diffraction maximum and a single diffuse-scattering component. The decomposition is especially important for diffraction maxima at low 2θ angles and in cases with severe line broadening (e.g., sample 4105, see Fig. 5b). If it was not possible to decompose the peak assuming a single phase (e.g., 400 peak of sample 4604, Fig. 5a), this peak was eliminated from the cell-parameter refinement. This first set of calculations provided good cell parameters for unzoned samples and an average cell parameter

TABLE 5. The 2θ (Cu$K\alpha$), intensity, and FWHM for Bragg and diffuse-scattering components of the 312 diffraction maxima

Sample no.	4403		4303				4601	
Peak no.*	A	B	A	B	C	D	A	D
2θ angle (°)	47.60	47.73	47.04	47.19	47.32	47.22	46.83	47.28
Intensity	1.5×10^3	9.9×10^2	6.5×10^2	6.4×10^2	1.5×10^2	1.6×10^3	3.0×10^3	3.7×10^3
FWHM (°)	0.11	0.13	0.09	0.06	0.05	0.35	0.63	1.02

* See Figure 4 and text for peak numbers.

for zoned crystals with split peaks. For samples with split peaks, a second refinement was completed assuming that the sample consisted of two phases. Diffraction maxima were determined by decomposing the curve with respect to Bragg diffraction maxima on the low- and the high-2θ side of the composite peak. Unit-cell parameters were refined separately using both sets of diffraction maxima. Thus, there are three sets of unit-cell parameters for the samples that had split peaks.

The results for unzoned and zoned samples (assuming a single phase) are compared with the data of Holland and Gottfried (1955) in Figure 6. As expected, unit-cell parameters increase with increasing α-decay dose. Below doses of 3×10^{15} α-decay events/mg, both a and c increase rapidly. Above doses of 3×10^{15} α-decay events/mg, a ceases to increase but c continues to increase. The error (indicated by the bars in Fig. 6) in the unit-cell parameters increases substantially at doses in excess of 3×10^{15} α-decay events/mg because of a decrease in intensity and broadening of the diffraction maxima. Thus, refined unit-cell parameters have limited value at doses above 3×10^{15} α-decay events/mg. Our results for the increase in unit-cell parameter with increasing α-decay dose are nearly identical to those of Holland and Gottfried (1955) at doses less than 3×10^{15} α-decay events/mg, but a significant difference occurs at higher values. Most notably, our results (although with large errors) suggest that at higher doses c continues to increase, whereas Holland and Gottfried suggested that c had reached a saturation value. The differences in the positions of our curve as compared with that of Holland and Gottfried may be as large as 0.002 nm for a and 0.005 nm for c at 8×10^{15} α-decay events/mg.

The refined unit-cell parameters are affected by whether the diffuse-scattering component is included from the peak profile (Murakami et al., 1986). Because the Bragg diffraction maximum is located on the low-2θ side of the asymmetric peaks, unit-cell parameters that do not include the diffuse-scattering component are larger than those that include the diffuse-scattering component (Fig. 7; see also Table 1, Murakami et al., 1986). This is not a significant effect at doses less than 3×10^{15} α-decay events/mg, as the Bragg maxima are sharp with little diffuse scattering. At higher α-decay doses the effect is significant because the diffuse-scattering component can nearly equal the Bragg component in its intensity. The differences in refined unit-cell parameters with and without the diffuse-scattering component reach values of 0.002 nm for a and 0.004 nm for c at a saturation dose of 8×10^{15} α-decay events/mg. This is approximately equal to the difference between the unit-cell parameters in this study and those of Holland and Gottfried (1955). Additionally, this may in part explain the discrepancy between unit-cell volume increases and swelling determined by dilatometric measurements of α-decay damaged material (Clinard et al., 1984; Weber and Maupin, 1988). The swelling measured in dilatometric measurements includes both the unit-cell expansion and the volume change associated with the crystalline-to-amorphous transition.

The expansion of the unit-cell parameters with increasing α-decay dose is compared with the results for the Pu-doped zircon (Weber, 1990, 1991) in Figure 8. For the Pu-doped zircon, the unit-cell parameters were not determined beyond a dose of 2×10^{15} α-decay events/mg because of broadening and the decrease in intensity of the diffraction maxima. The increase in the unit-cell parameters of the Pu-doped zircon is greater but closely parallels those for natural zircon. The increase in c with increasing α-decay dose for the Pu-doped zircon follows an exponential function $(1 - e^{-BD}$, in which B is a rate constant for simultaneous annealing of point defects and D is the dose) for natural zircon that is predicted by models for the simple accumulation of isolated defects (Nellis, 1977; Weber, 1981, 1982). The expansion along the **a** axis for the Pu-doped zircon is also apparently exponential; however, for natural zircon, there is a significant suppression of the expansion along the **a** axis at dose levels below 1×10^{15} α-decay events/mg that gives rise to the

TABLE 6. The 2θ (for Cu$K\alpha$), intensity, and FWHM for selected diffraction maxima

Sample no.	4604				4105		
Peak no.*	A	B	C	D	A	B	C
2θ angle (°)	55.22	55.40	55.55	55.57	52.48	53.08	53.58
Intensity	9.2×10^2	4.9×10^2	3.6×10^2	3.0×10^2	5.7×10^2	1.1×10^3	1.8×10^3
FWHM (°)	0.42	0.13	0.14	0.47	0.66	0.78	0.62

* See Figure 5 for peak numbers.

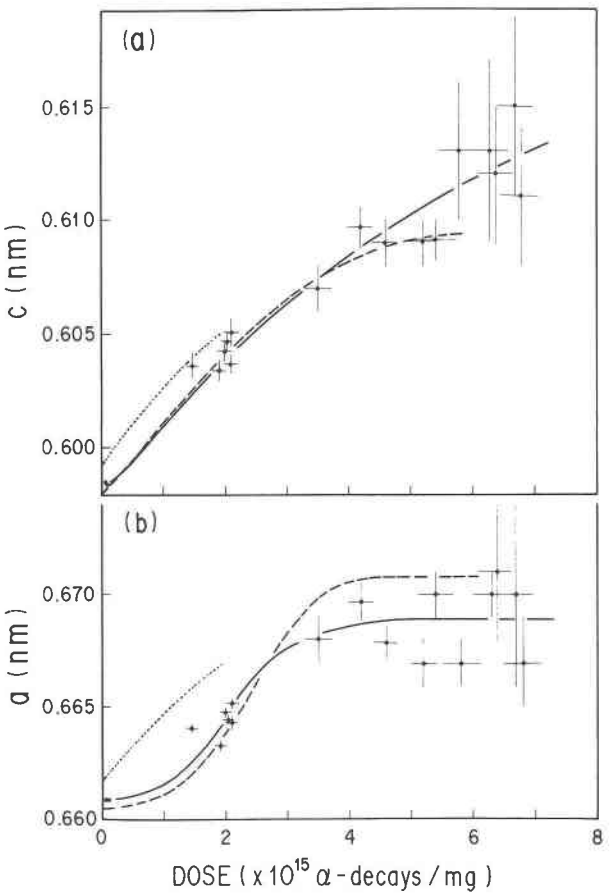

Fig. 6. Plot of change in (**a**) c and (**b**) a unit-cell parameters of zircon with increasing α-decay dose (assuming an age of 570 m.y.). The solid line is based on samples from this study; the dashed line, natural zircon (Holland and Gottfried, 1955); dotted line, Pu-doped zircon (Weber, 1990). Standard error is indicated by the length of the error bars. Unit-cell parameters are given in Table 8.

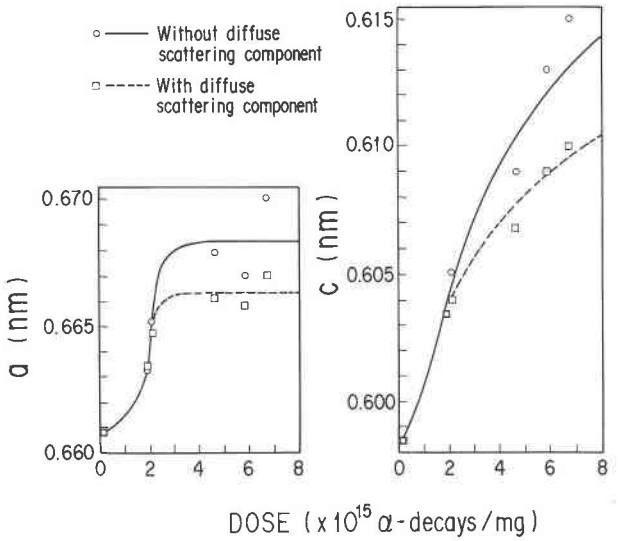

Fig. 7. Selected unit-cell parameters refined without the diffuse-scattering component (solid line) and with the diffuse-scattering component (dashed line). Original data are given in Murakami et al. (1986).

sigmoidal shape of the curve in Figure 6b. For natural zircon, $\Delta a/a_0$ is apparently suppressed relative to $\Delta c/c_0$ (Fig. 8). In contrast, there is a nearly linear relationship between $\Delta a/a_0$ and $\Delta c/c_0$ for the Pu-doped zircon, in good agreement with the observations of Crawford and Wittels (1956) on a neutron-irradiated single crystal of zircon (Fig. 8). The unit-cell expansion in natural zircon is anisotropic ($c > a$), and the saturation value for $\Delta a/a_0$ is 1.5%. The saturation value for $\Delta c/c_0$ is more difficult to assess because of the size of the error in the determination of c at high α-decay doses. Nevertheless, the saturation value for $\Delta c/c_0$ is greater than that reported by Holland and Gottfried (1955), 1.8%. This suggests that in natural zircon, annealing of defects over geologic periods of time results in relaxation of the expansion along the **a** axis. Holland and Gottfried (1955) noted similar behavior in a comparison of zircon from other localities and concluded that the Sri Lankan zircon in their study probably underwent some thermal recovery over geologic time. The timing and duration of the thermal event cannot be estimated.

The change in unit-cell volume of the samples in this study with increasing α-decay dose follows an empirical expression (Weber, 1990) of the form

$$\Delta V_{uc}/V_o = A_{uc}\{1 - \exp[-(B_{uc}D)^n]\} \quad (4)$$

where A_{uc} is the unit-cell volume change at saturation, B_{uc} is related to the rate constant (per unit dose) for simultaneous annealing of Frenkel defects during irradiation, and n is an order parameter that produces sigmoidal rather than simple exponential behavior. The values for A_{uc}, B_{uc}, and n have been determined by nonlinear regression analysis and are summarized in Table 4, along with values determined previously (Weber, 1990) for the Pu-doped zircon and for the data of Holland and Gottfried (1955).

In summary, the X-ray diffraction analysis reveals a

TABLE 7. Apparent zoning and peak splitting for samples examined by both optical microscopy and X-ray powder diffraction analysis

Sample no.	Dose ($\times 10^{15}$ α/mg)	Apparent zoning	Apparent peak splitting
4403	0.06	Yes	No
4606	1.46	Yes	Yes
4603	1.92	No	No
4602	2.01	No	Yes
4303	2.1	No	Yes
4601	4.6	Yes	No*
4501	5.4	Yes	No
4304	5.8	No	No
4104	6.4	Yes	No
4103	6.7	Yes	No

* It is usually difficult to decompose peaks for samples having doses higher than 4 × 10^{15} α/mg.

TABLE 8. Calculated unit-cell parameters (nm) based on the assumptions of one phase and two phases

	One phase		Two phases*			
			Low phase		High phase	
Sample no.	*a*	*c*	*a*	*c*	*a*	*c*
4403	0.66085(2)**	0.59845(3)				
4407	0.66085(3)	0.59834(4)				
4606	0.6641(2)	0.6036(5)	0.6647(2)	0.6041(5)	0.6623(1)	0.6021(4)
4603	0.6633(2)	0.6034(4)				
4602	0.6648(2)	0.6042(4)	0.6653(2)	0.6047(4)	0.6635(2)	0.6033(3)
4605	0.6645(1)	0.6047(4)	0.6650(1)	0.6052(4)	0.6632(2)	0.6037(4)
4607	0.6642(3)	0.6037(4)	0.6647(3)	0.6039(6)	0.6627(5)	0.602(1)
4303	0.6652(2)	0.6051(6)	0.6658(3)	0.6056(6)	0.6641(3)	0.6039(6)
4604	0.668(1)	0.607(1)	0.667(1)	0.607(2)	0.664(1)	0.605(2)
4302	0.6696(8)	0.6097(9)				
4601	0.6679(7)	0.609(1)				
4204	0.667(1)	0.609(1)				
4501	0.670(1)	0.6091(9)				
4304	0.667(1)	0.613(3)				
4105	0.670(1)	0.613(4)	0.667(1)	0.616(3)	0.6628(2)	0.6105(4)
4104	0.671(3)	0.612(3)				
4103	0.670(4)	0.615(4)				
4102	0.667(2)	0.611(3)				

* See text for explanation.
** Calculated standard error for last digit is given in parentheses.

three-stage process: Stage I: $<3 \times 10^{15}$ α-decay events/mg. Bragg diffraction maxima decrease in intensity by a factor of 2 but remain sharp. The diffuse-scattering component is minor (several orders of magnitude less than the Bragg diffraction maximum). These maxima are symmetric but shift to lower values of 2θ that correspond to significant increases in the unit-cell volume (nearly 5%). Stage II: 3×10^{15} to 8×10^{15} α-decay events/mg. Bragg diffraction maxima significantly decrease in intensity by several orders of magnitude. The intensity of the diffuse-scattering component increases; thus, diffraction maxima broaden and become asymmetric. The rate and amount of unit-cell expansion is small. Stage III: $>8 \times 10^{15}$ α-decay events/mg. The samples are X-ray diffraction amorphous. Finally, although the unit-cell expansion of Pu-doped zircon closely parallels that of natural zircon with increasing α-decay dose, the sigmoidal shape of the curves clearly suggests a slight thermal recovery of isolated defects in the early stages of damage, particularly in the **a** direction.

HRTEM

Because of zoning and heterogeneities within individual zones, a wide variety of damaged microstructures was observed by HRTEM in even a single sample. Further, we were not able to determine U and Th concentrations quantitatively with the EDS on individual grains (less than 1 μm in size) dispersed on the holey carbon grid. Therefore, we estimated the α-decay dose based on the electron diffraction pattern. Qualitatively, the α-decay dose characteristic of each electron diffraction pattern can be determined by comparison with X-ray single-crystal diffraction patterns. Figure 9 shows the X-ray single-crystal diffraction pattern of a ($h0l$) plane as a function of increasing α-decay dose (up to 6.7×10^{15} α-decay events/mg). Note the intensity and spot size change not only as a function of the intensity of the incident beam and exposure time but also with the size of the crystals. Changes in the single-crystal diffraction pattern can be directly related to changes in the X-ray powder diffraction patterns (already described). Thus, we can use the electron diffraction pattern to characterize the stage of damage. Diffuse streaking and shifts in the diffraction spots (e.g., changes in unit-cell parameters) provide additional information. As an example, sample 4303 shows diffuse streaking of the 200 and $\bar{2}00$ maxima (arrows in Fig. 9c), suggesting that at doses between 2×10^{15} to 3×10^{15} α-decay events/mg the zircon may have a strained or distorted microstructure.

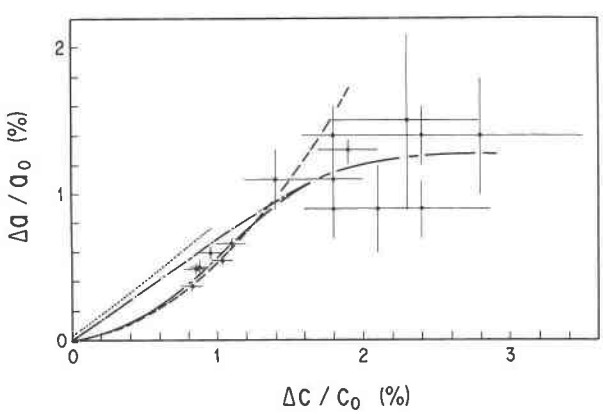

Fig. 8. Plot of the change in unit-cell parameter ($\Delta a/a$ vs. $\Delta c/c$). Zircon in this study, solid line and circles with standard error bars; natural zircon, dashed line (Holland and Gottfried, 1955); Pu-doped zircon, dotted line (Weber, 1990); neutron-irradiated zircon, dashed and dotted line (Crawford and Wittels, 1956).

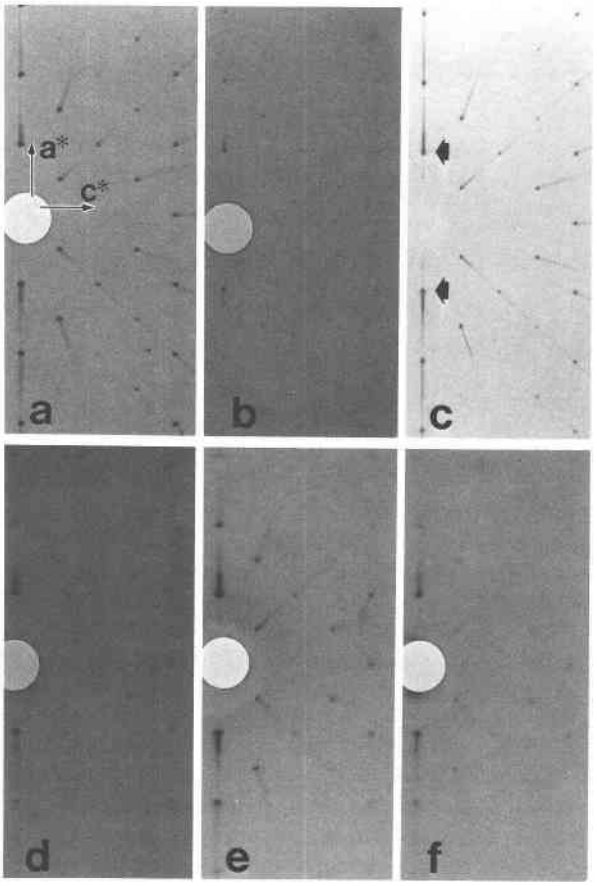

Fig. 9. Precession photographs (Mo/Zr) of the (*h*0*l*) plane of zircon as a function of increasing α-decay event dose up to dose of 6.7×10^{15} α-decay events/mg. **(a)** Sample 4403, 35 kV, 10 mA, 16.5 h; **(b)** 4603, 35 kV, 15 mA, 17 h; **(c)** 4303, 35 kV, 10 mA, 15 h; **(d)** 4601, 35 kV, 15 mA, 17 h; **(e)** 4304, 35 kV, 15 mA, 100 h; **(f)** 4103, 35 kV, 15 mA, 120 h.

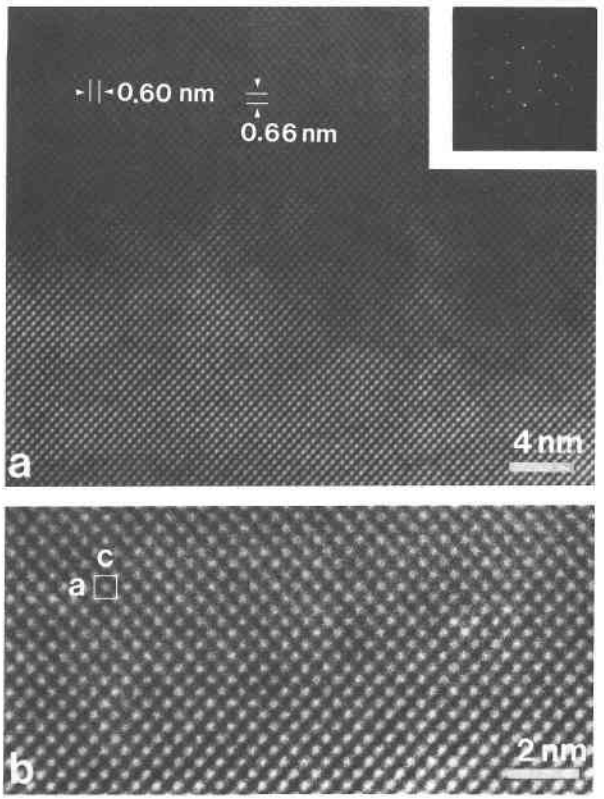

Fig. 10. **(a)** Two-dimensional lattice image in the (010) plane showing perfect lattice fringes and electron diffraction pattern. Principal lattice dimensions are given for the [100] (0.66 nm) and [001] (0.60 nm) directions. **(b)** Enlarged region of a portion of **a**. Unit cell is outlined.

Stage I microstructures and diffraction patterns are illustrated in Figures 10 through 12 as a function of increasing α-decay dose. Figure 10 shows perfect two-dimensional lattice fringes in the (010) plane, and the electron diffraction pattern is sharp. There are no distortions or discontinuities in the lattice fringes. Although the electron diffraction pattern in Figure 11 is sharp, a mottled diffraction contrast dominates the microstructure and lattice fringes are slightly distorted (arrow, Fig. 11a). There are isolated areas in which lattice fringes are absent (arrow, Fig. 11b). The size of the isolated areas in which fringes are absent ranges from 1 to 5 nm; the arrow (Fig. 11b) points to one of the smaller areas. Headley et al. (1982), in an ion-implantation study of zircon, estimated the diameter of a cylindrical-shaped, collision cascade to be on the order of 3 nm. Clinard (1986), in a study of ^{238}Pu-substituted zirconolite, assumed a spherical shape to the α-recoil track and from swelling results obtained a value of 5.4 nm. Assuming a total of 2000 atomic displacements for a single α-recoil nucleus, we obtain an estimated size of 2–5 nm. Based on the estimates of the size of individual α-recoil tracks, the isolated areas in which lattice fringes are absent may correspond to individual α-recoil tracks. In Figure 12, the mottled diffraction contrast, lattice fringe distortions and discontinuities, and the lattice-fringe-free domains become more evident, even though the electron diffraction pattern remains sharp. There are isolated instances of crystalline domains with high-angle grain boundaries. In stage I, misoriented crystallites are rarely seen. The streaking evident in the X-ray diffraction patterns (Fig. 9c) may correspond to the increased lattice fringe distortion and discontinuities. Thus, the microstructures in stage I can be characterized by increasing lattice-fringe distortion and an increase in lattice-fringe-free domains with increasing α-decay dose. Electron diffraction patterns remain sharp.

Stage II microstructures are illustrated in Figures 13 and 14. Electron diffraction maxima become broad and diffuse (Fig. 13), and aperiodic domains dominate the microstructure. Although two-dimensional lattice fringes are still evident in the crystalline domains, the electron diffraction pattern and the oriented crystalline domains (7–20 nm) suggest that the original zircon structure is still retained discontinuously over wide regions despite the

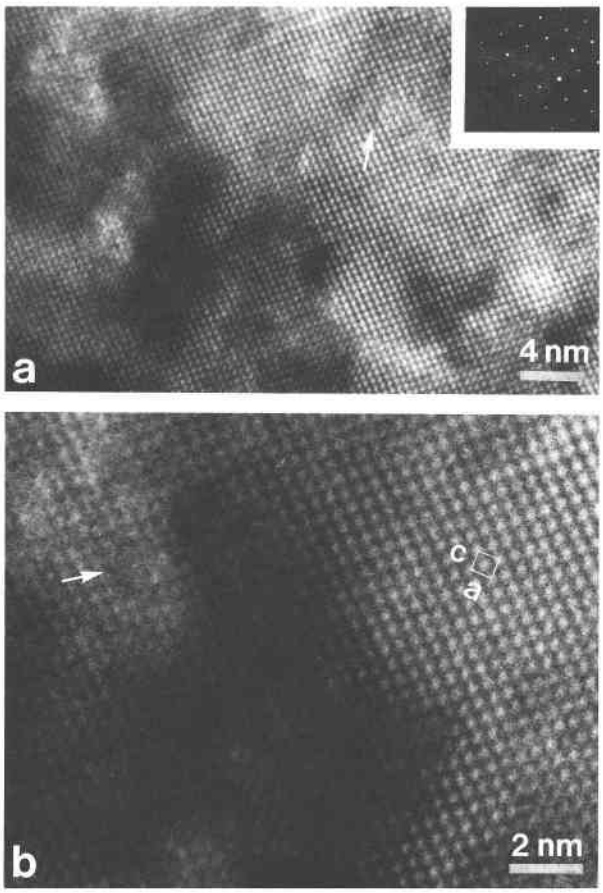

Fig. 11. (**a**) Two-dimensional lattice image in the (010) plane and electron diffraction pattern. Mottled diffraction contrast with slight distortion of the lattice fringes (arrow) is apparent. (**b**) Enlarged region of a portion of **a**. Aperiodic domains (1–5 nm) exist in which lattice fringes are indistinct or almost absent (arrow).

severe distortion and domain rotation. In Figure 14, microcrystallites (1–6 nm) are irregular in shape and share low-angle boundaries that have the same crystallographic orientation as the original structure. Diffraction patterns are often accompanied by faint, diffuse diffraction halos associated with the aperiodic regions. Thus, in stage II one may distinguish the degree of radiation damage by the ratio of aperiodic to crystalline volume.

In stage III, there is no evidence for long-range atomic periodicity (Fig. 15). The HRTEM image reveals an irregular contrast, and the electron diffraction pattern consists of a diffuse diffraction halo. This is similar to electron diffraction patterns obtained for other fully metamict phases (Lumpkin et al., 1986; Lumpkin and Ewing, 1988). The high-resolution image is consistent with the expected image for a random network model (Bursill et al., 1981). One of the unusual features of zircon is that high-dose samples have misoriented crystalline domains (1–10 nm) in the aperiodic matrix. The electron diffraction pattern for such microstructures consists of "spotty" rings with a diffuse diffraction halo from the aperiodic domains.

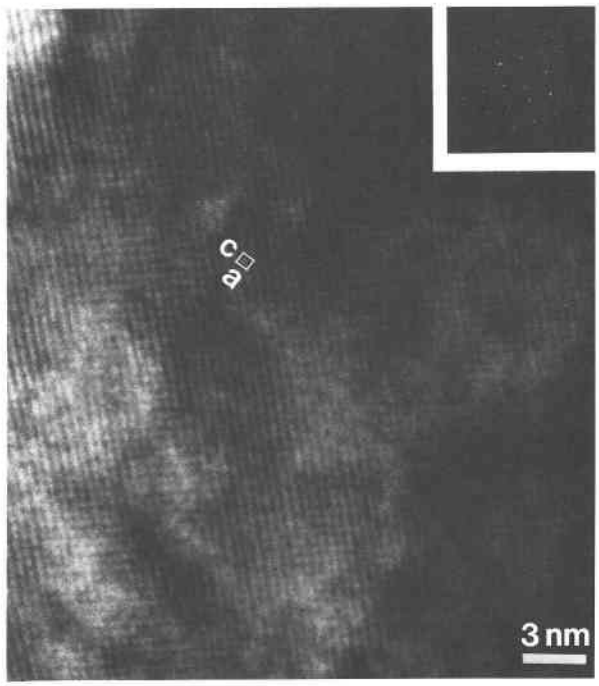

Fig. 12. Two-dimensional lattice image in the (010) plane and electron diffraction pattern. Lattice-fringe distortion and discontinuities become more apparent. Aperiodic domains increase in number and begin to overlap.

These crystallites are different from those observed in stage II in that the degree of misorientation is high, and in some cases the fragments of structure may be quite small. These fragments have been described as "a single column of the original structure" (Bursill and Thomas, 1981) and may be isolated, residual crystalline material not fully damaged to the aperiodic state, yet highly misoriented because of the large strain associated with the transition to the aperiodic state (15% volume change). Figure 16 demonstrates that lattice fringes occur in the aperiodic matrix even if axial-beam lattice imaging is used. The aperiodic matrix usually shows an irregular diffraction contrast (Fig. 16a). The braided, ropelike microstructure does not retain any long-range periodicity and gives no diffraction pattern characteristic of crystalline material (Fig. 16b). The left corners of Figures 16a and 16b have microcrystallites that correspond to the powder ring in the inset of Figure 16a.

In summary, the three stages of damage determined on the basis of powder X-ray diffraction data can be easily distinguished by HRTEM. Still, the heterogeneity in the distribution of U and Th in the samples means that even for high-dose samples (4103, 6.7×10^{15} α-decay events/mg) crystalline regions are found, and for low dose samples (4407, 0.075×10^{15} α-decay events/mg) aperiodic regions may be found. For zoned samples (4601, 4.6×10^{15} α-decay events/mg) examples of each of the three stages of damage may be seen (Chakoumakos et al., 1987). In sample 4601, the dose covers the range from $2.0 \times$

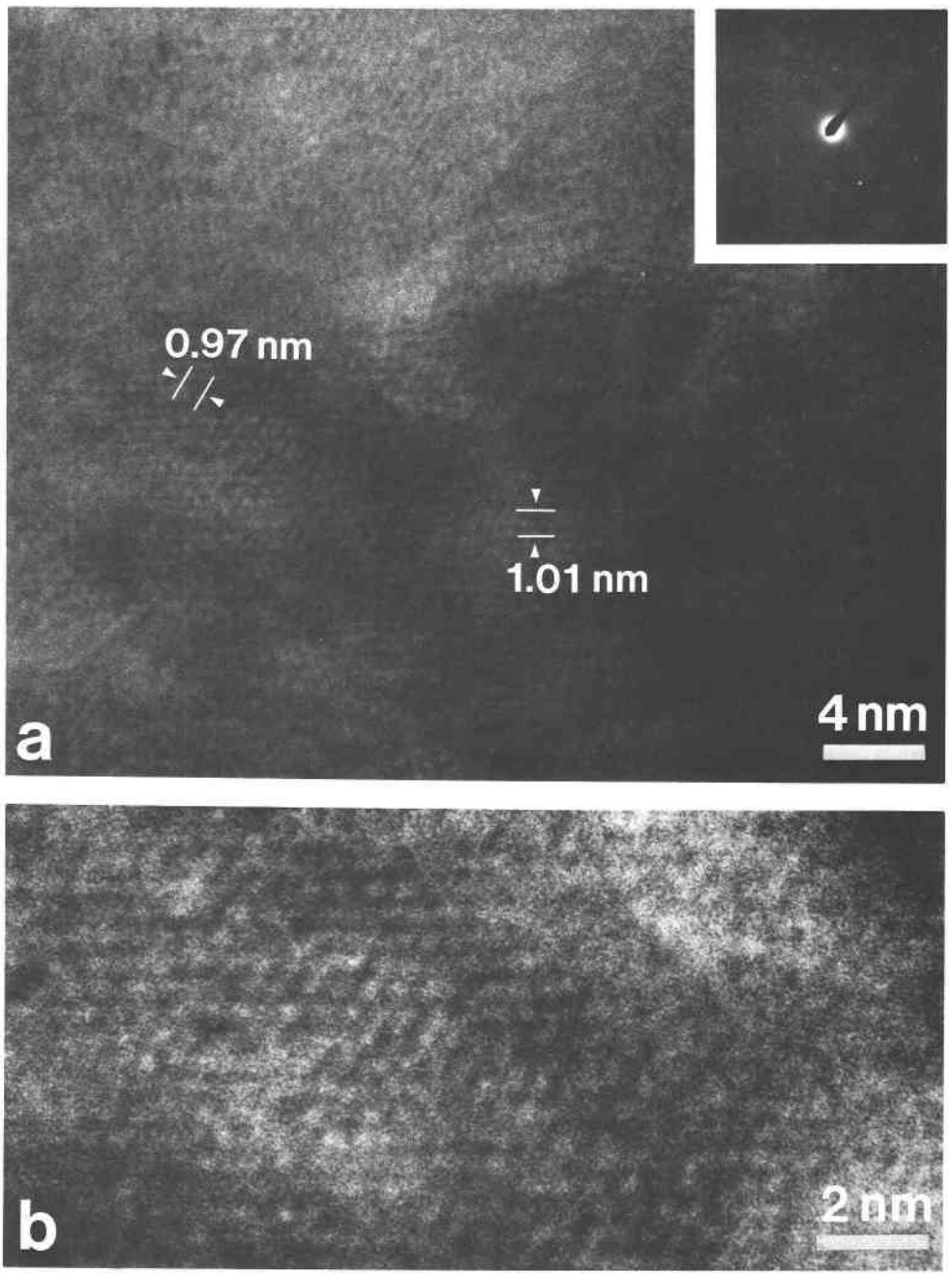

Fig. 13. (**a**) Lattice-fringe image normal to $[\bar{1}11]$ and electron diffraction pattern. The diffraction pattern changes remarkably; spots are broad and diffuse, and there are faint powder rings. Lattice fringes are more distorted and discontinuous. Large regions of the original structure remain, although crystalline domains (7–20 nm) also persist. Aperiodic domains are abundant. Lattice dimensions are given for the [110] (1.01 nm) and $[0\bar{1}1]$ (0.97 nm) directions. (**b**) Enlarged region of a portion of **a**. Two-dimensional lattice fringes may still be recognized.

10^{15} to 8.0×10^{15} α-decay events/mg, essentially the full range of doses over which the crystalline to metamict transformation occurs.

Annealing kinetics

To investigate the origin of the highly misoriented crystallites, ten grains of zircon (4103, 6.7×10^{15} α-decay events/mg) were annealed in situ in the electron microscope at 750 °C. Prior to thermal treatment, the electron diffraction patterns consisted of diffuse diffraction halos, faint powder rings, or broad, faint diffraction maxima (the variation in diffraction pattern is the result of heterogeneities in the distribution of U and Th). After 2 d at temperature, no change was observed in the diffraction patterns. There was no evidence for the formation of the misoriented crystallites. This behavior is consistent with

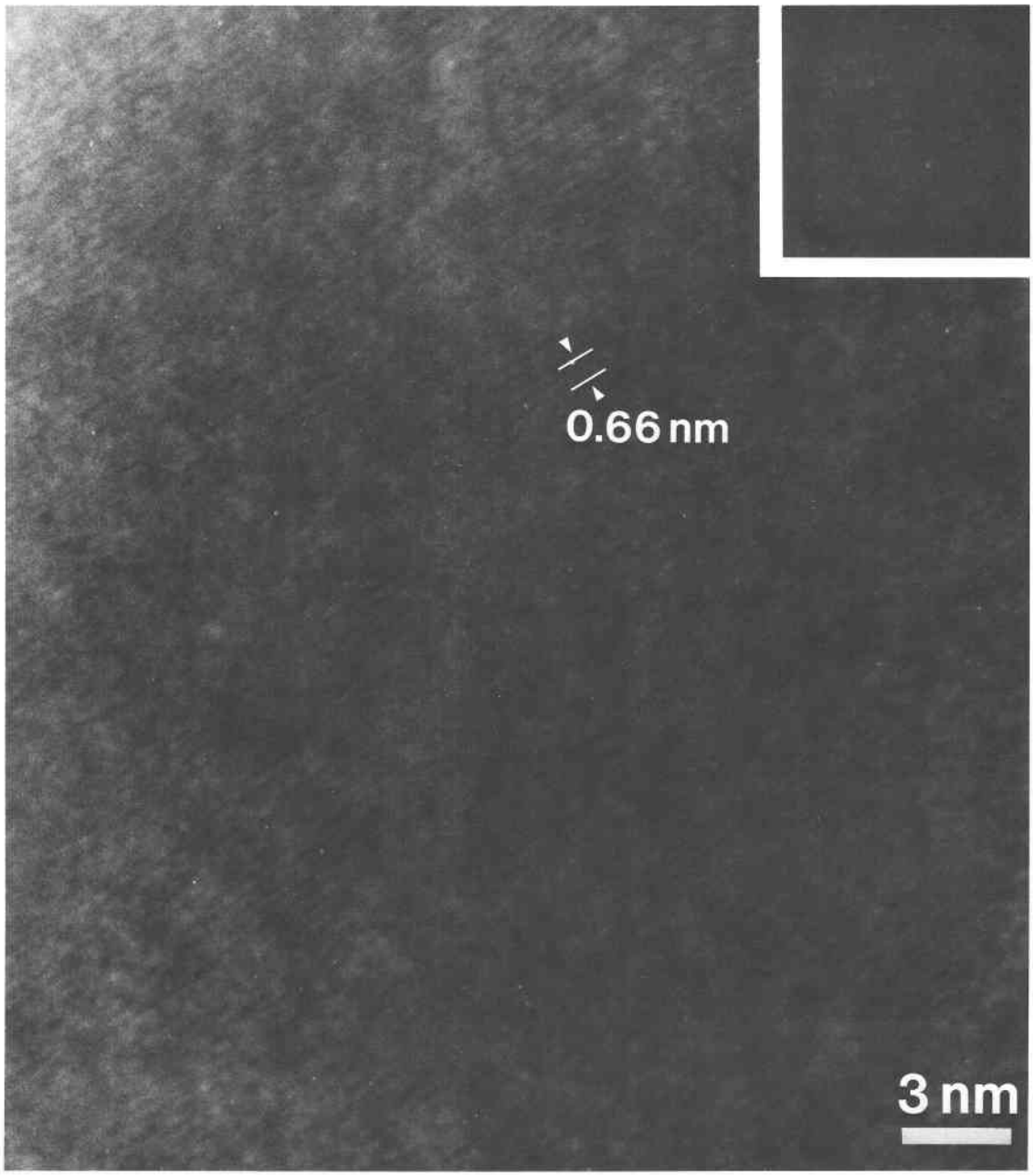

Fig. 14. Lattice-fringe image parallel to [100] and electron diffraction pattern. Lattice dimension is given for the [100] (0.66 nm) direction. Crystalline and aperiodic domains have almost equal volumes. Microcrystallites (1–6 nm), irregular in shape and sharing indistinct boundaries with the matrix, have the same crystallographic orientation as the original structure. Diffraction spots are broad, and a faint diffraction halo is apparent.

recent observations of Pu-doped zircon (Weber, 1990, 1991) in which recrystallization of the aperiodic state required annealing at temperatures exceeding 1000 °C.

Discussion

Alpha-decay damage accumulation

X-ray and electron diffraction analysis allow the definition of the three-stage damage process that is illustrated in Figure 17. The X-ray powder diffraction pattern (left column), the single-crystal X-ray and electron diffraction patterns (center column), and the schematic structural changes (right column) are shown as a function of increasing α-decay dose (top to bottom). Figure 17a illustrates the diffraction patterns characteristic of the fully crystalline zircon.

Stage I, Figure 17b ($<3 \times 10^{15}$ α-decay events/mg), is characterized by Bragg powder diffraction maxima that decrease in intensity by a factor of 2 but remain sharp. The diffuse-scattering component is minor (several or-

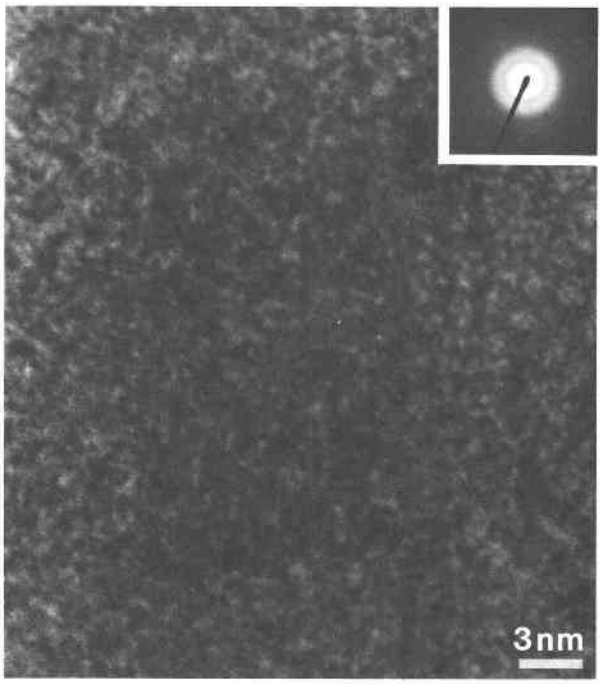

Fig. 15. High-resolution image and electron diffraction pattern of completely damaged, aperiodic region. No lattice fringes are evident, and there are no powder rings in the diffraction pattern.

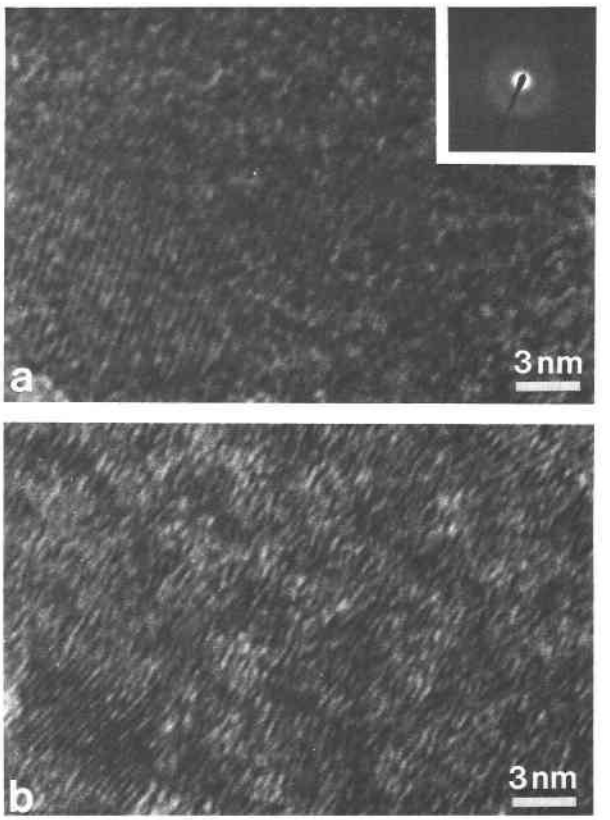

Fig. 16. Lattice-fringe images and electron diffraction pattern of the aperiodic matrix: (**a**) typical and (**b**) less common textures.

ders of magnitude less than the Bragg diffraction maximum). The diffraction maxima are symmetric but shift to lower values of 2θ that correspond to significant increases in the unit-cell volume (nearly 5%). HRTEM shows a characteristic mottled diffraction contrast and isolated lattice-fringe free domains (1–5 nm). The volume fraction of the aperiodic domains appears to be less than 20%. The mottled diffraction contrast is the result of elastic strain fields around defect clusters formed by interstitial defects (Bursill and McLaren, 1966). The decrease in Bragg diffraction intensity (by a factor of 2), despite the slight distortion of the lattice fringes and the limited abundance of aperiodic domains, may result from the effect of the strain fields on coherent scattering from atoms in the volumes affected.

Stage II, Figures 17c and 17d (3×10^{15} to 8×10^{15} α-decay events/mg), shows drastic changes in the zircon structure. The Bragg diffraction maxima significantly decrease in intensity by several orders of magnitude. The intensity of the diffuse-scattering component increases (Fig. 17c), and the diffraction maxima broaden and become asymmetric. The rate and amount of unit-cell expansion is small. Aperiodic domains increase in volume and show significant overlap with one another. The decrease in diffraction intensity is mainly the result of the decrease in the volume of diffracting, crystalline material. At higher doses, Figure 17d, the aperiodic domains dominate the structure. X-ray and electron diffraction patterns do not change except for the decrease in diffraction intensity and broadening of diffraction spots (Fig. 9, center column of Figs. 17c and 17d). Thus, the original zircon structure is retained without any change in orientation despite the accumulation of substantial volumes of aperiodic material.

At stage III, Figure 17e ($>8 \times 10^{15}$ α-decay events/mg), zircon is X-ray and electron diffraction amorphous. This three-stage process does not involve the formation of crystallites (e.g., zircon, ZrO_2 or SiO_2) or different, derivative structure types, as has been reported for zirconolite, $CaZrTi_2O_7$, at intermediate doses (Ewing and Headley, 1983). One should note that misoriented crystallites are present (see Fig. 16). The fraction seen by HRTEM is limited; therefore, their formation is not explicitly indicated in the schematic of the damage process (Fig. 17). It is possible that they are part of the process of damage accumulation, but they could also be the result of (1) annealing resulting from beam heating, (2) long-term annealing of damage (recrystallization), (3) recrystallization associated with a later thermal event, or (4) low-temperature alteration. Our results suggest that misoriented crystallites are quite limited in volume and would not be detected by X-ray diffraction techniques.

The three-stage process clearly delineates the damage effects of the α-particle and the α-recoil nucleus. The increase in the cell parameters is the main feature of stage

I; the increase in the volume of aperiodic domains associated with the α-recoil nucleus is the main feature of stage II. Interstitial defects are most important in stage I (inducing lattice strain); the collision cascades, creating larger volumes of aperiodic material, are most important in stage II. Thus, one expects a difference in the annealing kinetics associated with each type of defect. This sequence of damage accumulation has also been described for pyrochlore structure types (Krivokoneva and Sidorenko, 1971; Lumpkin and Ewing, 1988). Both of these studies used diffraction maxima line broadening to demonstrate that strain is the most important effect in stage I and that the decrease in grain size (increase of aperiodic regions) is the most important feature of stage II. HRTEM micrographs of stage II (Fig. 13) show that the periodic domains can have severe distortions even when the crystallite size is small. At the highest doses associated with stage II, one expects and observes (Lumpkin and Ewing, 1988) a decrease in strain as defects migrate to the aperiodic sink and the proportion of crystalline, strained material decreases.

This analysis of the damage accumulation process allows one to distinguish among three different states for the zircon. At each stage of damage, the zircon will consist of different proportions of (1) crystalline, undistorted zircon ("phase 2" of Holland and Gottfried, 1955), (2) damaged or distorted crystalline zircon, and (3) aperiodic zircon. The fully crystalline zircon probably only occurs at doses less than 0.5×10^{15} α-decay events/mg. Unit-cell distortion (diffraction maxima shift to lower values of 2θ) occurs primarily in stage I, and afterwards the diffraction maxima show only negligible shift. Thus, at stage II, α-decay damaged zircon consists of three regions: (1) undamaged, undistorted crystalline material, (2) distorted crystalline material with expanded unit-cell parameters, and (3) completely aperiodic regions. The volume fractions of these regions may be represented by the following relation:

$$f_c + f_{cd} + f_a = 1 \quad (5)$$

where f_c, f_{cd}, and f_a are the volume fractions of perfectly crystalline, distorted crystalline, and aperiodic regions, respectively. Therefore,

$$\rho_{bulk} = f_c\rho_c + f_{cd}\rho_{cd} + f_a\rho_a. \quad (6)$$

Changes in the overall bulk density are given by

$$\Delta\rho/\rho_0 = f_c\Delta\rho_c/\rho_0 + f_{cd}\Delta\rho_{cd}/\rho_0 + f_a\Delta\rho_a/\rho_0 \quad (7)$$

where ρ_{bulk}, ρ_c, ρ_{cd}, and ρ_a are bulk density, crystalline density, distorted crystalline density, and the aperiodic density, respectively. Note, $\Delta\rho_c/\rho_0 = 0$.

At stage II, there is no evidence for any substantial volume of undamaged crystalline material, f_c, remaining. This is based on two observations: (1) At stage II, there is no further expansion of the unit cell as evidenced by continued shifts in the position of diffraction maxima to lower values of 2θ. (2) Direct observation by HRTEM does not show any substantial volume of undistorted, perfectly crystalline material remaining. This is an important point because Holland and Gottfried (1955) modeled the changes in density, refractive index, and the diffraction maxima intensities in terms of varying proportions of three phases. Phase 2 (f_2 in their calculation) consisted of undistorted, perfectly crystalline zircon, which became most prominent at intermediate doses (our stage II). This phase 2 never showed any unit-cell expansion and passed directly into the metamict state at higher α-decay doses. Holland and Gottfried (1955) suggested that the microstructure of phase 2 played a critical role in determining whether a material became metamict. If the crystallites of phase 2 were disoriented, as in the case of zircon, the material readily broke down to the metamict state. If the crystallites remained oriented with respect to the original structure, the material self-annealed and did not become metamict. An alternative explanation of their observations is that the zircon that was modeled to have contained phase 2 at intermediate doses was actually zoned zircon. At intermediate doses, zones with low U and Th contents would still be crystalline and would not show a unit-cell expansion as the bulk α-decay dose increased. At lower doses, all zones would be crystalline, and thus no phase 2 would be present. At higher doses, all zones would be aperiodic. Only at intermediate doses does one still expect to find crystalline zones. This would explain why phase 2 did not undergo increased unit-cell

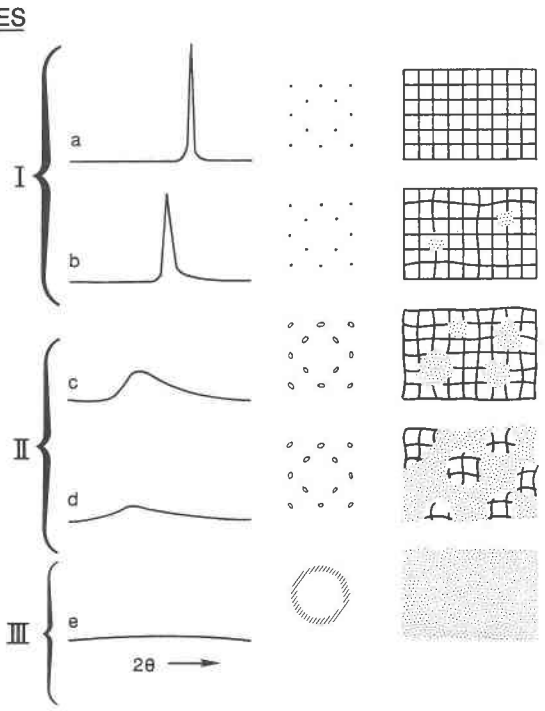

Fig. 17. Schematic representation of the change in X-ray diffraction pattern (left column), electron diffraction pattern (center column), and structure (right column) with increasing α-decay dose (top to bottom).

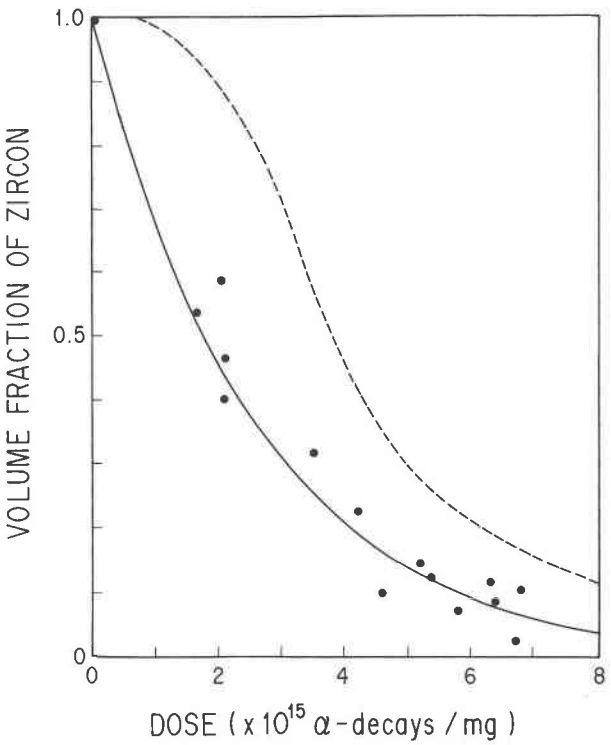

Fig. 18. Volume fraction of crystalline material in natural zircon estimated assuming that it is proportional to the Bragg diffraction intensity (I/I_0) as a function of α-decay event dose. The dashed line is based on refractive indices (Holland and Gottfried, 1955).

expansion with increasing α-decay dose and occurred at stage II. This interpretation is certainly consistent with our X-ray diffraction data in which there was no evidence for any perfectly crystalline zircon remaining. If phase 2 were present (Holland and Gottfried suggested as much as 30%), it would be clearly evident from the intensity and position of diffraction maxima at intermediate α-decay doses.

Thus, at stage II, in the absence of any significant proportion of undamaged crystalline material, the previous relations reduce to

$$f_{cd} + f_a = 1 \tag{8}$$

$$\rho_{bulk} = f_{cd}\rho_{cd} + f_a\rho_a \tag{9}$$

$$\Delta\rho/\rho_0 = f_{cd}\Delta\rho_{cd}/\rho_0 + f_a\Delta\rho_a/\rho_0. \tag{10}$$

The bulk densities have been measured (Table 2), and the densities of the distorted crystalline regions, ρ_{cd}, may be calculated from the unit-cell parameters (Table 8). Distortion parameters as a function of dose are not known for the crystalline domains (Krivoglaz, 1969); thus f_{cd} was estimated assuming that it is proportional to I/I_0, where I was the intensity of a diffraction maximum for the sample and I_0 was the intensity of the diffraction maximum for a crystalline standard. The 312 diffraction maxima were used to calculate f_{cd} for each sample. (Samples 4403 and 4407 were used as the crystalline standards.) A first-order exponential dependence was assumed and the data fitted to the curve shown in Figure 18. A similar set of calculations was made using the 200 diffraction maxima, and consistent results were obtained. For 312 maxima, $k = 3.9 \times 10^{-16}$ mg/α-decay event; 200, $k = 4.2 \times 10^{-16}$ mg/α-decay event for the relation

$$I/I_0 = \exp(-kD) \tag{11}$$

where D = α-decay event dose.

The volume fractions of distorted crystalline zircon based on X-ray intensities (Fig. 18) is less than one would expect from the HRTEM micrographs. Thus, X-ray diffraction intensities provide a poor estimate of the volume fraction of crystalline material because (1) the X-ray diffraction intensities are greatly affected by lattice distortion (Krivoglaz, 1969), and (2) we have assumed a first-order exponential dependence rather than a sigmoidal dependence. Holland and Gottfried (1955) estimated the volume fraction of crystalline zircon using refractive indices, and their estimate (Fig. 18) is in better qualitative agreement with the estimates from HRTEM in this study. Weber (1990), using his analysis of X-ray diffraction data for Pu-doped zircon, also concluded that X-ray diffraction intensities do not provide the best estimate of the volume of crystalline material.

Using both estimates (I/I_0 and refractive indices) for the volume fraction of crystalline material, f_{cd}, the densities of the aperiodic domains, ρ_a, were calculated. (Bulk density, ρ_{bulk}, was measured, and the density of crystalline zircon, ρ_{cd}, was calculated from X-ray diffraction data.) Figure 19 shows the density changes for bulk zircon (solid line), distorted crystalline zircon (dashed line), and aperiodic zircon (dotted line). There is no major difference in the position of the line that represents the change in the density of aperiodic zircon, regardless of whether I/I_0 (open circles) or refractive indices (squares) are used. The density change of the distorted crystalline zircon is a direct result of the expansion of the unit cell, and this expansion ceases at doses greater than 3×10^{15} α-decay events/mg. Thus, these domains do not undergo significant change during stage II while they are being converted to aperiodic regions by α-recoil damage. In contrast, the density of the aperiodic regions continues to decrease with increasing dose. At the beginning of stage II, the modeled density is 4.5 g/cm^3, and at the end of stage II it is 4.1 g/cm^3. Thus, redamage of aperiodic regions causes continued adjustments at the atomic level. This is also evident when one compares changes in properties of the bulk specimens. Lumpkin and Ewing (1988) have already noted that density continues to decrease even after a material becomes X-ray and electron diffraction amorphous. Clinard (1986) has also called attention to the fact that structural rearrangements in aperiodic materials continue with increasing α-decay dose in Pu-doped zirconolite. One should note, however, that this modeled range of densities for the aperiodic regions in zircon assumes that there are no remaining, undamaged crystalline regions (as pro-

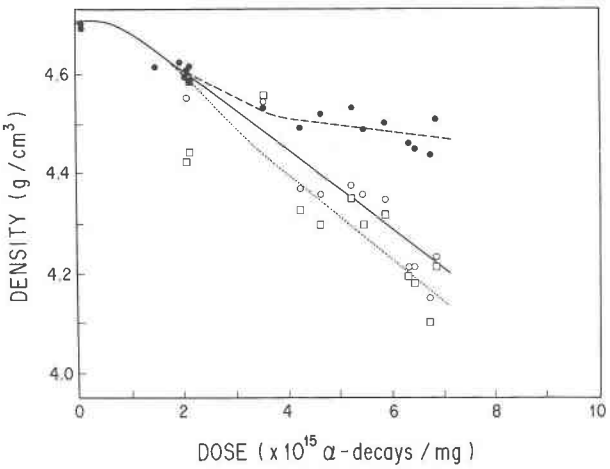

Fig. 19. Density changes in bulk zircon (solid line), crystalline zircon (dashed line), and aperiodic zircon (dotted line) as a function of increasing α-decay dose. Density values for the crystalline zircon are calculated from the refined unit-cell parameters (solid circles). Density values for the aperiodic zircon are based on X-ray diffraction intensities, I/I_0, (open circles) and refractive indices (squares) after Holland and Gottfried (1955).

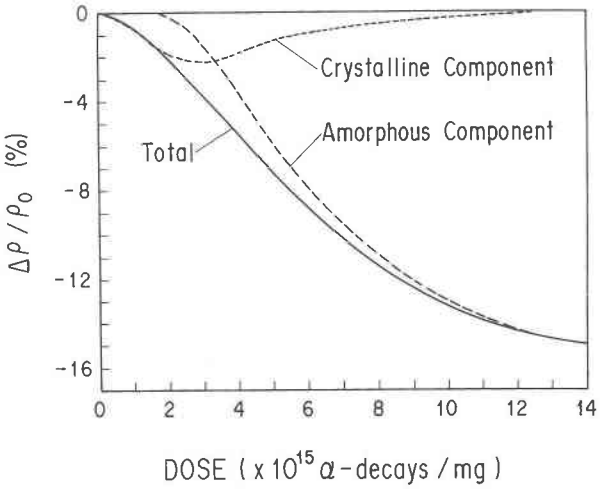

Fig. 20. Crystalline and amorphous contributions to the overall density change for zircon in this study based on a double-overlap model for amorphization and fitted expressions to the measured unit-cell expansion and density change (after the method of Weber, 1990).

posed by Holland and Gottfried, 1955). To the extent that such undamaged regions are present, the range of modeled densities is narrower.

Weber (1990, 1991) analyzed the damage accumulation process in both Pu-doped zircon and natural zircon (using the data of Holland and Gottfried, 1955). One may model amorphization as the result of the accumulation of single displacement cascades or as the result of overlapping individual displacement cascades. Such models have been used to consider direct and multiple overlap processes in the accumulation of amorphous volumes in ion-irradiated semiconductors. We do not review these models or repeat Weber's analysis in this paper (the reader is referred to Weber, 1990), but we note the following important results: (1) The X-ray diffraction amorphous state is reached at 6.7×10^{15} α-decay events/mg for Pu-doped zircon. (2) The sigmoidal shape of the damage curves for natural zircon suggests an incubation dose (9.89×10^{14} α-decay events/mg) prior to the onset of significant disorder and amorphization. (3) The accumulation of aperiodic material is best modeled by a double-overlap model that indicates a limiting local defect concentration is required to trigger amorphization. (4) Based on the double-overlap model, the total mass of material damaged in a single collision cascade of a recoil nucleus is 5.84×10^{-19} g, equivalent to several thousand atomic displacements (for Pu-doped zircon) and 5.89×10^{-19} g (for natural zircon, using the data of Holland and Gottfried). (5) The overall macroscopic swelling can be separated into contributions from unit-cell expansion of crystalline components and volume expansion associated with the crystalline-to-amorphous transition within overlapped recoil-nuclei tracks. Volume expansion is clearly dominated by unit-cell expansion at low doses. (6) Isochronal annealing showed a sharp recovery in density associated with recrystallization that suggests a narrow range for the densities of the aperiodic regions.

Although the data range is more limited, an analysis similar to that summarized above (Weber, 1990) has been applied to the density data for samples in this study. The double-overlap model provides a reasonable fit to the derived amorphous fraction and yields values of 9.27×10^{14} α-decay events/mg for the incubation dose and 3.31×10^{-19} g for the mass of material damaged per α-decay event (in the collision cascade of a recoil nucleus). The incubation dose is in good agreement with the analysis cited above for the data of Holland and Gottfried. The mass of material damaged per decay event is almost a factor of 2 less than that determined for the data of Holland and Gottfried and the Pu-doped zircon; however, the lack of high-dose data in the present study precludes an accurate determination of this value. Based on this analysis, the overall macroscopic density change, $\Delta\rho/\rho$, can be separated into crystalline and amorphous contributions, as shown in Figure 20. These results clearly illustrate the composite nature of the radiation damage process. In the early stages of α-decay damage, the density decrease is clearly dominated by contributions from the unit-cell expansion. At higher α-decay doses, the change in density is most affected by the crystalline-to-amorphous transformation and perhaps by a continued decrease in the density of the aperiodic regions as they are redamaged.

Fission fragment damage

No fission fragment tracks were observed in the zircon from Sri Lanka, and fission fragment tracks have not been reported in a number of radiation damaged zircon sam-

ples (Headley et al., 1981; Headley et al., 1986; Headley and Ewing, 1986; Chan and Buseck, 1982). However, Yada et al. (1981, 1987) produced high-resolution images of fission fragment tracks in zircon using a 1000 kV high-resolution electron microscope. The absence of fission tracks in our samples suggests that fission-event damage is not an important part of the radiation-induced transformation to the metamict state. In fact, one would not expect fission fragment damage to be as important as α-decay damage because of the small number of fission events in the decay series of ^{235}U, ^{238}U, and ^{232}Th. Thus, contrary to the suggestion of Yada et al. (1981, 1987) and Speer (1982), fission fragment damage is not an important contributor to the radiation-induced transformation from the periodic to aperiodic state.

Annealing kinetics

The final structure of a material that suffers radiation damage depends not only on the rate of damage accumulation but also on the kinetics of the annealing process. The balance between these two competing processes determines the microstructure at any given point in the history of the sample. The crystallinity in natural radiation-damaged zircon may be restored on heating. Bursill and McLaren (1966) annealed partially damaged (but still crystalline) zircon over a range of temperatures of 750 °C (15 h) to 1250°C (15 h) and examined the samples using HRTEM. The single-crystal character of the zircon specimen was restored but with the formation of dislocation loops. None of the samples in their study, however, had reached stage III in damage. We performed an in situ annealing study (750 °C for two d) with the electron microscope on a sample well advanced into stage II damage (6.7×10^{15} α-decay events/mg). No evidence for annealing or the formation of crystallites was observed. This suggests that for fully damaged zircon, the annealing rate must be very slow. This has been substantiated in recent studies on Pu-doped zircon (Weber, 1990) that clearly established that recrystallization of fully damaged zircon required annealing at temperatures exceeding 1000 °C.

Still, there is evidence for annealing under ambient conditions and over geologic periods of time. We have already noted that fission tracks are rare or absent in the Sri Lankan zircon. Fission tracks are retained in zircon up to temperatures of 200 °C ± 50 °C (Fleischer et al., 1965; Krishnaswami et al., 1974; Fleischer et al., 1975; Gleadow and Brooks, 1979); thus, fission track damage is more easily annealed in zircon than are α-recoil tracks. This confirms our conclusion that fission fragment damage is not an important part of the metamictization process. This also suggests that the zircon may have experienced some recent thermal event that removed the fission tracks and perhaps led to the formation of the misoriented microcrystallites. Based on neutron irradiation experiments, Vance and Anderson (1972) also suggested that Sri Lankan zircon has been thermally annealed. Further, Lumpkin and Ewing (1988) have shown that, in general, the α-decay dose required for the formation of the metamict state increases with the age of the zircon samples. A corrected dose may be calculated assuming exponential decay of the α-recoil track with time. A corrected dose (one displacement per atom = saturation of damage) requires an assumed mean life for an α-recoil track in zircon of 400 m.y. Although such an estimate can only be considered qualitative because the thermal histories of ancient zircon are generally not known, the evidence for annealing is compelling.

Perhaps the clearest demonstration of annealing effects is in the comparison of the damage curves for ^{238}Pu-doped zircon (6.5 yr old) and natural zircon (570 m.y. old) shown in Figure 1. At low doses, the unit-cell volume expansion is greater for the Pu-doped zircon than the natural zircon ($<3 \times 10^{15}$ α-decay events/mg), and the decrease in density is greater for Pu-doped zircon than the natural zircon ($<6 \times 10^{15}$ α-decay events/mg). This suggests thermal recovery of isolated defects that are characteristic of stage I damage and more limited recovery of damage at stage II (recrystallization of individual α-recoil tracks). For both synthetic and natural zircon, the curves for density change vs. α-decay dose converge at high α-decay doses (stage III), suggesting no measurable recrystallization of the amorphous material over geologic periods of time. Indeed, in the double-overlap model of Weber (1990), the incubation dose required before the onset of amorphization in natural zircon is attributed to the annealing of defects over geologic periods of time. From kinetic considerations (for samples of great age, i.e., 10^6 yr) one would expect a measurable fraction of defect annealing at 20 °C for simple (point) defects with activation energies in the range of 1.5 eV. This is the range of activation energies for annealing of isolated defects in simple oxides (Clinard and Hobbs, 1986).

Conclusions

Based on X-ray diffraction analysis and HRTEM, three stages of damage accumulation may be delineated. In stage I ($<3 \times 10^{15}$ α-decay events/mg), damage is dominated by the accumulation of isolated point defects that cause unit-cell expansion and distortion. These defects may anneal over geologic periods of time. Stage II (3×10^{15} to 8×10^{15} α-decay events/mg) consists of crystalline regions with point defects and amorphous tracks caused by overlapped α-recoil nuclei. With increasing α-decay dose, damaged crystalline regions are converted into aperiodic regions, but there is no further expansion of the unit cell in the remaining crystalline regions. Stage III ($>8 \times 10^{15}$ α-decay events/mg) consists of material that is entirely aperiodic as far as can be determined by X-ray or electron diffraction. Contrary to previous suggestions (Pellas, 1965; Lipova et al., 1965), there is no evidence for the formation of ZrO_2 or SiO_2 as final products during the last stage of metamictization (Farges and Calas, 1991). Based on modeled density changes, the density of damaged, aperiodic regions continues to decrease as these areas are redamaged at increasing α-decay doses. These calculations suggest that during stage II of the process, the den-

sity of aperiodic regions changes from 4.5 g/cm^3 to 4.1 g/cm^3. The change in density may be less if crystalline, undamaged zircon is still present. Fission fragment damage does not contribute to the process of metamictization. The amorphization process is consistent with a model for the multiple overlap of displacement cascades, suggesting amorphization occurs as a result of defect accumulation rather than directly within a displacement cascade.

Comparison of results for natural zircon with those for Pu-doped zircon shows that dose-rate effects (even as great as a factor of 10^8) have no substantial effect on the damage accumulation process. This is an important observation because it means that actinide-doping experiments can be used to simulate the long-term effects of radiation damage on nuclear waste form phases. Slight differences in changes in unit-cell parameters and density between Pu-doped and natural zircon with increasing α-decay dose do, however, suggest that annealing of point defects in the early stages of the damage accumulation process occurs in natural zircon under ambient conditions. This accounts for the distinct sigmoidal shape of the damage curves for natural zircon and the apparent incubation period before the onset of amorphization.

Acknowledgments

This work was supported by the U.S. Department of Energy, Office of Basic Energy Sciences, under grant no. DE-FG04-84ER45099 with the University of New Mexico (R.C.E.), Contract DE-AC05-840R21400 with Martin Marietta Energy Systems, Inc. (Oak Ridge National Laboratory), and Contract DE-AC06-76RL0 1830 with Battelle Memorial Institute. Electron microprobe analysis and the electron microscopy were completed in the Microbeam Analysis Facility of the Department of Geology, UNM, supported by NSF, NASA, BES, and the State of New Mexico. The instrumental neutron activation analyses were completed at Los Alamos National Laboratory by the Research Reactor Group through the generous efforts of S.R. Garcia (Los Alamos National Laboratory) and H.E. Newsom (UNM). R.C.E. thanks the Japan Atomic Energy Research Institute and the INE/Kernforschungszentrum Karlsruhe for the support and time to finish this manuscript.

References cited

Ahrens, L.H., Cherry, R.D., and Erlank, A.J. (1967) Observations on the Th-U relationship in zircons from granitic rocks and from kimberlites. Geochimica et Cosmochimica Acta, 31, 2379–2387.

Aines, R.D., and Rossman, G.R. (1986) Relationships between radiation damage and trace water in zircon, quartz, and topaz. American Mineralogist, 71, 1186–1193.

Albee, A.L., and Ray, L. (1970) Correction factors for electron microanalysis of silicates, oxides, carbonates, phosphates and sulfates. Analytical Chemistry, 42, 1408–1414.

Appleman, D.C., and Evans, H.T., Jr. (1973) Indexing and least-squares refinement of powder diffraction data, National Technical Information Service, Document PB-216, 188 p.

Bence, A.E., and Albee, A.L. (1968) Empirical correction factors for the electron microanalysis of silicates and oxides. Journal of Geology, 76, 382–403.

Bursill, L.A., and Braunshausen, G. (1990) Heavy-ion irradiation tracks in zircon. Philosophical Magazine A, 62, 395–420.

Bursill, L.A., and McLaren, A.C. (1966) Transmission electron microscope study of natural radiation damage in zircon ($ZrSiO_4$). Physica Status Solidi, 13, 331–343.

Bursill, L.A., and Thomas, J.M. (1981) High-resolution electron microscopy of microscrystalline, partially crystalline, and amorphous silicates. Journal of Physical Chemistry, 85, 3007–3010.

Bursill, L.A., Mallinson, L.G., Elliott, S.R., and Thomas J.M. (1981) Computer simulation and interpretation of electron microscopic images of amorphous structures. Journal of Physical Chemistry, 85, 3004–3006.

Cartz, L., and Fournelle, R. (1979) Metamict zircon formed by heavy ion bombardment. Radiation Effects, 41, 211–217.

Chakoumakos, B.C., Murakami, T., Lumpkin, G.R., and Ewing, R.C. (1987) Alpha-decay induced fracturing in zircon: The transition from the crystalline to the metamict state. Science, 236, 1556–1559.

Chan, I.Y., and Buseck, P.R. (1982) Metamictization in zircon. In G.W. Bailey, Ed., Proceedings of the 40th Annual Meeting of the Electron Microscopy Society of America, p. 618–619. San Francisco Press, Inc., San Francisco.

Clinard, F.W., Jr. (1986) Review of self-irradiation effects in Pu-substituted zirconolite. American Ceramic Society Bulletin, 65, 1181–1187.

Clinard, F.W., Jr, and Hobbs, L.W. (1986) Radiation effects in non-metals. In R.A. Johnson and A.N. Orlov, Eds., Physics of radiation effects in crystals, p. 387–471. North-Holland, New York.

Clinard, F.W., Jr., Rohr, D.L., and Roof, R.B. (1984) Structural damage in a self-irradiated zirconolite-based ceramic. Nuclear Instruments and Methods in Physics Research, B1, 581–586.

Crawford, J.H., and Wittels, M.C. (1956) A review of investigations of radiation effects in covalent and ionic crystals. In Proceedings of International Conference on Peaceful Uses of Atomic Energy, vol. 7, p. 654–665. United Nations, New York.

Dahanayake, K., and Ranasinghe, A.P. (1981) Source rocks of gem minerals: Case study from Sri Lanka. Mineralium Deposita, 16, 103–111.

Davis, G.L., Hart, S.R., and Tilton, G.R. (1968) Some effects of contact metamorphism on zircon ages. Earth and Planetary Science Letters, 5, 27–34.

Ewing, R.C. (1975) The crystal chemistry of complex niobium and tantalum oxides IV. The metamict state: Discussion. American Mineralogist, 60, 728–730.

Ewing, R. C., and Headley, T.J. (1983) Alpha-recoil damage in natural zirconolite ($CaZrTi_2O_7$). Journal of Nuclear Materials, 119, 102–109.

Ewing, R.C., Haaker, R.F., and Lutze, W. (1983) Leachability of natural zircon, $ZrSiO_4$, as a function of α-dose. In W. Lutze, Ed., Scientific basis for radioactive waste management V, Materials Research Society Proceedings, vol. 11, p. 389–398. North-Holland, New York.

Ewing, R.C., Chakoumakos, B.C., Lumpkin, G.R., and Murakami, T. (1987) The metamict state. Materials Research Society Bulletin, 12, 58–66.

Exarhos, G.J. (1984) Induced swelling in radiation damaged $ZrSiO_4$. Nuclear Instruments and Methods in Physics Research, B1, 538–541.

Farges, F., and Calas, G. (1991) Structural analysis of radiation damage in zircon and thorite: An X-ray absorption spectroscopic study. American Mineralogist, 76, 60–73.

Faure, G. (1977) Principles of isotope geology. Wiley, New York.

Fleischer, R.L., Price, P.B., and Walker, R.M. (1965) Effects of temperature, pressure and ionization on the formation and stability of fission tracks in minerals and glasses. Journal of Geophysical Research, 70, 1497–1502.

——— (1975) Nuclear tracks in solids. University of California Press, Berkeley, California.

Gentry, R.V. (1984) Lead retention in zircons. Science, 223, 835.

Gentry, R.V., Sworski, T.J., McKown, H.S., Smith, D.S., Eby, R.E., and Christie, W.H. (1982) Differential lead retention in zircons: Implications for nuclear waste containment. Science, 216, 296–298.

Gleadow, A.J.W., and Brooks, C.K. (1979) Fission track dating, thermal histories and tectonics of igneous intrusions in East Greenland. Contributions to Mineralogy and Petrology, 71, 45–60.

Gorz, H. (1974) Microprobe studies of inclusions and compilation of minor and trace elements in zircons from the literature. Chemie der Erde, 33, 326–357.

Gottfried, D., Senftle, F.E., and Waring, C.L. (1956) Age determination of zircon crystals from Ceylon. American Mineralogist, 41, 157–161.

Hamberg, A. (1914) Die radioaktiven Substanzen und die geologische Forschung. Geologiska Föreningens Stockholm Förhandlingar, 36, 31–96.

Harker, A.B., and Flintoff, J.F. (1984) Polyphase ceramic and glass-ceramic forms for immobilizing ICPP high-level nuclear waste. In G.L.

McVay, Ed., Scientific basis for nuclear waste management VII, vol. 26, p. 513–520. North-Holland, New York.
Headley, T.J., and Ewing, R.C. (1986) TEM study of the microstructure of metamict minerals. Microanalysis—1986, p. 141–144. San Francisco Press, San Francisco.
Headley, T.J., Ewing, R.C., and Haaker, R.F. (1981) High resolution study of the metamict state in zircon. In G.W. Bailey, Ed., Proceedings of the 1981 Annual Meeting of the Electron Microscopy Society of America, p. 112–113. Claitor's Publishing Division, Baton Rouge.
Headley, T.J., Arnold, G.W., and Northrup, C.J.M. (1982) Dose-dependence of Pb-ion implantation damage in zirconolite, hollandite, and zircon. In W. Lutze, Ed. Scientific basis for radioactive waste management V, vol. 11, p. 379–388. North-Holland, New York.
Headley, T.J., Ewing, R.C., and Haaker, R.F. (1986) TEM study of the metamict state. In R.I. Kostov and B.K. Kamenov, Eds., Physics of minerals and ore microscopy, p. 281–289. Bulgarian Academy of Science, Sofia, Bulgaria.
Holland, H.D., and Gottfried, D. (1955) The effect of nuclear radiation on the structure of zircon. Acta Crystallographica, 8, 291–300.
Holland, H.D., and Kulp, J.L. (1950) Geologic age from metamict minerals. Science, 111, 312.
Howard, C.J., and Sabine, T.M. (1974) X-ray diffraction profiles from neutron-irradiated magnesium oxide. Journal of Physical Chemistry: Solid State Physics, 7, 3453–3466.
Hurley, P.M., and Fairbairn, H.W. (1952) Alpha-radiation damage in zircon. Journal of Applied Physics, 23, 1408.
——— (1953) Radiation damage in zircon: A possible age method. Bulletin of the Geological Society of America, 64, 659–673.
Jäger, E., and Hunziker, J.C. (1979) Lectures in isotope geology. Springer-Verlag, Berlin.
Krishnaswami, S., Lal, D., Prabhu, N., and MacDougall, D. (1974) Characteristics of fission tracks in zircon: Applications to geochronology and cosmology. Earth and Planetary Science Letters, 22, 51–59.
Krivoglaz, M.A. (1969) Theory of X-ray and thermal-neutron scattering by real crystals. Plenum Press, New York.
Krivokoneva, G.K., and Sidorenko, G.A. (1971) The essence of the metamict transformation in pyrochlores. Geochemistry International, 8, 113–122.
Kröner, A., Williams, I.S., Compston, W., Baur, N., Vitanage, P.W., and Perrera, L.R.K. (1987) Zircon ion microprobe dating of high-grade rocks in Sri Lanka. Journal of Geology, 95, 775–791.
Lipova, I.M., Kuznetsova, G.A., and Markarov, Ye.S. (1965) An investigation of the metamict state in zircons and cyrtolites. Geochemistry International, 2, 513–525 (translated from Geokhimiya, no. 6, 681–694, 1965).
Ludwig, K.R., Zartman, R.E., and Goldich, S.S. (1984) Lead retention in zircons. Science, 223, 835.
Lumpkin, G.R., and Chakoumakos, B.C. (1988) Chemistry and radiation effects of thorite-group minerals from the Harding pegmatite, Taos County, New Mexico. American Mineralogist, 73, 1405–1419.
Lumpkin, G.R., and Ewing, R.C. (1988) Alpha-decay damage in minerals of the pyrochlore group. Physics and Chemistry of Minerals, 16, 2–20.
Lumpkin, G.R., Ewing, R.C., Chakoumakos, B.C., Greegor, R.B., Lytle, F.W., Foltyn, E.M., Clinard, F.W., Jr., Boatner, L.A., and Abraham, M.M. (1986) Alpha-recoil damage in zirconolite ($CaZrTi_2O_7$). Journal of Materials Research 1, 564–576.
Minor, M.M., Hensley, W.K., Denton, M.M., and Garcia, S.R. (1982) An automated activation analysis system. Journal of Radioanalytical Chemistry, 70, 459–471.
Munasinghe, T., and Dissanayake, C.B. (1981) The origin of gemstones of Sri Lanka. Economic Geology, 76, 1216–1225.
Murakami, T., Chakoumakos, B.C., and Ewing, R.C. (1986) X-ray powder diffraction analysis of alpha-event radiation damage in zircon ($ZrSiO_4$). In D.E. Clark, W.B. White, and J. Machiels, Eds., Advances in ceramics: Nuclear waste management II, vol. 20, p. 745–753. American Ceramic Society, Columbus, Ohio.
Nellis, W.J. (1977) The effect of self-radiation on crystal volume. Inorganic and Nuclear Chemistry Letters, 13, 393–398.
Pabst, A. (1952) The metamict state. American Mineralogist, 37, 137–157.
Pellas, P. (1965) Etude sur la recristallisation thermique des zircons metamictes. Memoires du Museum National d'Historie Naturelle, Serie C, Sciences de la Terre, 12, 227–253.
Peterman, Z.E., Zartman, R.E., and Sims, P.K. (1986) A protracted Archean history in the Watersmeet Gneiss Dome, northern Michigan. U.S. Geological Survey Bulletin, 1622, 51–64.
Petit, J.-C., Dran, J.-C., and Della Mea, G. (1987) Effects of ion implantation on the dissolution of minerals. Part II: Selective dissolution. Bulletin francaise de Minéralogie et de Cristallographie, 110, 25–42.
Pidgeon, R.T., O'Neil, J.R., and Silver, L.T. (1966) Uranium and lead isotopic stability in a metamict zircon under experimental hydrothermal conditions. Science, 154, 1538–1540.
Sahama, T.G. (1981) Growth structure in Ceylon zircon. Bulletin francaise de Minéralogie et de Crystallographie, 104, 89–94.
Silver, L.T. (1964) The relation between radioactivity and discordance in zircons. National Research Council Publication 1075, 34–39.
Silver, L.T., and Deutsch, S. (1963) Uranium-lead isotopic variations in zircons: A case study. Journal of Geology, 71. 721–758.
Speer, J.A. (1982) Zircon. In Mineralogical Society of America Reviews in Mineralogy, 5, 67–112.
Stackelberg, M.v., and Rottenback, E. (1940a) Dichte und Struktur des Zirkons III. Zeitschrift für Kristallographie, 102, 173–182.
——— (1940b) Dichte und Struktur des Zirkons IV. Zeitschrift für Kristallographie, 102, 207–208.
Steiger, R.H., and Wasserburg, G.J. (1966) Systematics in the Pb^{208}-Th^{232}, Pb^{207}-U^{235}, and Pb^{206}-U^{238} systems. Journal of Geophysical Research, 71, 6065–6090.
Suzuki, K. (1987) Discordant distribution of U and Pb in zircon of Naegi granite: A possible indication of Rn migration through radiation damage. Geochemical Journal, 21, 173–182.
Tole, M.P. (1985) The kinetics of dissolution of zircon ($ZrSiO_4$). Geochimica et Cosmochimica Acta, 49, 453–458.
Vance, E.R., and Anderson, B.W. (1972) Study of metamict Ceylon zircons. Mineralogical Magazine, 38, 605–613.
Wayne, D.M., and Sinha, A.K. (1988) Physical and chemical response of zircons to deformation. Contributions to Mineralogy and Petrology, 98, 109–121.
Weber, W.J. (1981) Ingrowth of lattice defects in alpha irradiated UO_2 single crystals. Journal of Nuclear Materials, 98, 206–215.
——— (1982) Radiation damage in a rare-earth silicate with the apatite structure. Journal of the American Ceramic Society, 65, 544–548.
——— (1983) Radiation-induced swelling and amorphization in $Ca_2Nd_8(SiO_4)_6O_2$. Radiation Effects, 77, 295–308.
——— (1984) Alpha-irradiation damage in CeO_2, UO_2 and PuO_2. Radiation Effects, 83, 145–156.
——— (1990) Radiation-induced defects and amorphization in zircon. Journal of Materials Research, 5, 2687–2697.
——— (1991) Self-radiation damage and recovery in Pu-doped zircon. Radiation Effects and Defects in Solids, 115, 341–349.
Weber, W.J., and Matzke, Hj. (1986) Radiation effects in actinide host phases. Radiation Effects 98, 93–99.
Weber, W.J., and Maupin, G.D. (1988) Simulation of radiation damage in zircon. Nuclear Instruments and Methods in Physics Research, B32, 512–515.
Weber, W.J., Wald, J.W., and Matzke, Hj. (1986) Effects of self-radiation damage in Cm-doped $Gd_2Ti_2O_7$ and $CaZrTi_2O_7$. Journal of Nuclear Materials, 138, 196–209.
Wittels, M.C., and Sherrill, F.A. (1954) Radiation damage in SiO_2 structures. Physical Review, 93, 1117–1118.
Woodhead, J.A., Rossman, G.R., and Silver, L.T. (1991) The metamictization of zircon: Radiation dose-dependent structural characteristics. American Mineralogist, 76, 74–82.
Yada, K., Tanji, T., and Sunagawa, I. (1981) Application of lattice imagery to radiation damage investigation in natural zircon. Physics and Chemistry of Minerals, 7, 47–52.
——— (1987) Radiation induced lattice defects in natural zircon ($ZrSiO_4$) observed at atomic resolution. Physics and Chemistry of Minerals, 14, 197–204.

Manuscript received September 11, 1990
Manuscript accepted May 23, 1991